Nano Energy 89 (2021) 106461

Contents lists available at ScienceDirect

Nano Energy

journal homepage: www.elsevier.com/locate/nanoen

Review

Nanogenerator-based devices for biomedical applications

Mingjun Sun [a,b,1], Zhe Li [a,c,1], Chunyu Yang [a,b], Yujia Lv [a], Lin Yuan [a,b], Chenxi Shang [a,b], Shiyuan Liang [a,e], Bowen Guo [a,b], Yan Liu [d,*], Zhou Li [a,e,f,**], Dan Luo [a,e,f,**]

[a] CAS Center for Excellence in Nanoscience, Beijing Key Laboratory of Micro-nano Energy and Sensor, Beijing Institute of Nanoenergy and Nanosystems, Chinese Academy of Sciences, Beijing 101400, PR China
[b] State Key Laboratory of Heavy Oil Processing, College of New Energy and Materials, Beijing Key Laboratory of Biogas Upgrading Utilization, China University of Petroleum (Beijing), Beijing 102249, PR China
[c] Institute of Engineering Medicine, School of Life Science, Beijing Institute of Technology, Beijing 100081, PR China
[d] Laboratory of Biomimetic Nanomaterials, Department of Orthodontics, Peking University School and Hospital of Stomatology, Beijing 100081, PR China
[e] School of Nanoscience and Technology, University of Chinese Academy of Sciences, Beijing 100049, PR China
[f] Center on Nanoenergy Research, School of Physical Science and Technology, Guangxi University, Nanning 530004, PR China

ARTICLE INFO

Keywords:
Triboelectric nanogenerator
Piezoelectric nanogenerator
Medical applications
Self-powered
Implanted and wearable devices

ABSTRACT

Microelectronics, as indispensable tools in clinics, can monitor physiological signals, treat diseases, and promote human health. An efficient and uninterrupted energy supply is key to the application of implanted and wearable devices. Traditional energy supply systems typically rely on batteries and connections to external power sources; however, the inconvenience of charging, limited working life of the battery, and the risk of reoperation limit their applications, and meanwhile prompt investigation of self-driven, long-term power supplies. The nanogenerator, as an ideal power supply, collects biomechanical energy from physiological activities such as muscle movement, heartbeat, respiration, gastric peristalsis, and performs electrical signal conversion for detection of physiological/pathological indicators, cardiac pacing, nerve stimulation, tissue repair, and weight control. Here, we review the design of nanogenerators and their biomedical applications, which may inspire future development of self-powered medical devices.

1. Introduction

The continuous development and application of electronics and advanced materials has promoted use of implantable and wearable electronic products [1–3], such as devices implanted *in vivo* (pacemaker [4], neurostimulator [5–7]), smart watches [8], glasses [9], and bracelets [10–12]. Although electronic devices have achieved great success, they face many challenges [13–15]. In medical applications, to ensure normal operation of implanted devices in vivo, they must be small and have high flexibility, sensitivity, and mechanical stability [16,17]. A continuous power supply is key for the reliability of electronic devices [18–20]. Traditional power supply systems, relying on batteries and external power sources, have the disadvantages of large size, high energy consumption, short service life, and need for regular replacement, which increase the economic, physical, and psychological burden on patients [21]. To overcome these limitations, the development of a self-powered electrical energy harvesting system with high biocompatibility and durability is important for medical electronic devices.

In 2006, Professor Zhong-Lin Wang invented the world's first piezoelectric nanogenerator (PENG) based on a ZnO nanowire array, which generates an electric field by piezoelectric polarization and drives the movement of electrons, converting mechanical energy into electricity [22]. Piezoelectric nanogenerators are used in energy harvesters, sensors, wearable devices, and medical implants [23,24]. The initial piezoelectric materials were typically ZnO [25–29], lead zirconate titanate (PZT) [30–36], barium titanate (BT) [37–41], and polyvinylidene fluoride [42–45]. Subsequently, organic piezoelectric biomaterials—such as protein nanofiber membranes [46], M13 phage membranes [47], and piezoelectric peptide nanostructures were developed [48,49]. In 2012, Professor Zhong-Lin Wang developed a

* Corresponding author.
** Corresponding authors at: CAS Center for Excellence in Nanoscience, Beijing Key Laboratory of Micro-nano Energy and Sensor, Beijing Institute of Nanoenergy and Nanosystems, Chinese Academy of Sciences, Beijing 101400, PR China.
E-mail addresses: orthoyan@bjmu.edu.cn (Y. Liu), zli@binn.cas.cn (Z. Li), luodan@binn.cas.cn (D. Luo).
[1] These authors contribute equally.

https://doi.org/10.1016/j.nanoen.2021.106461
Received 17 July 2021; Received in revised form 19 August 2021; Accepted 22 August 2021
Available online 26 August 2021

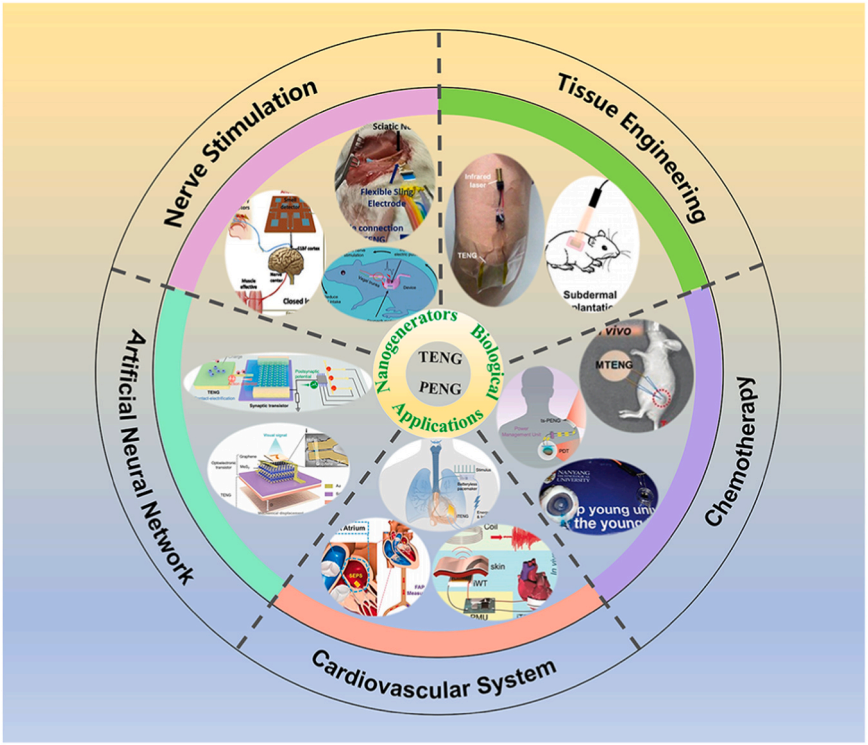

Fig. 1. Biomedical applications of nanogenerator-based devices.

triboelectric nanogenerator (TENG) based on the principles of triboelectricity and electrostatic induction, in which the electrostatic charge generated by the contact interface of different materials forms an electric field and drives the movement of electrons [50]. TENG has higher output power and energy conversion efficiency and allows universal selection of materials. Because friction is common in daily life, the TENG can collect energy from natural environments such as human activity [51–53], water droplets [54–58], airflow [59,60], ocean waves and tides [60–64], enabling a wide range of applications. At present, TENG is mainly used in blue energy utilization [65–67], human-computer interaction [68–71], wearable electronic devices [72–76], electronic skins [77–80], and implantable medical devices [81,82]. In terms of

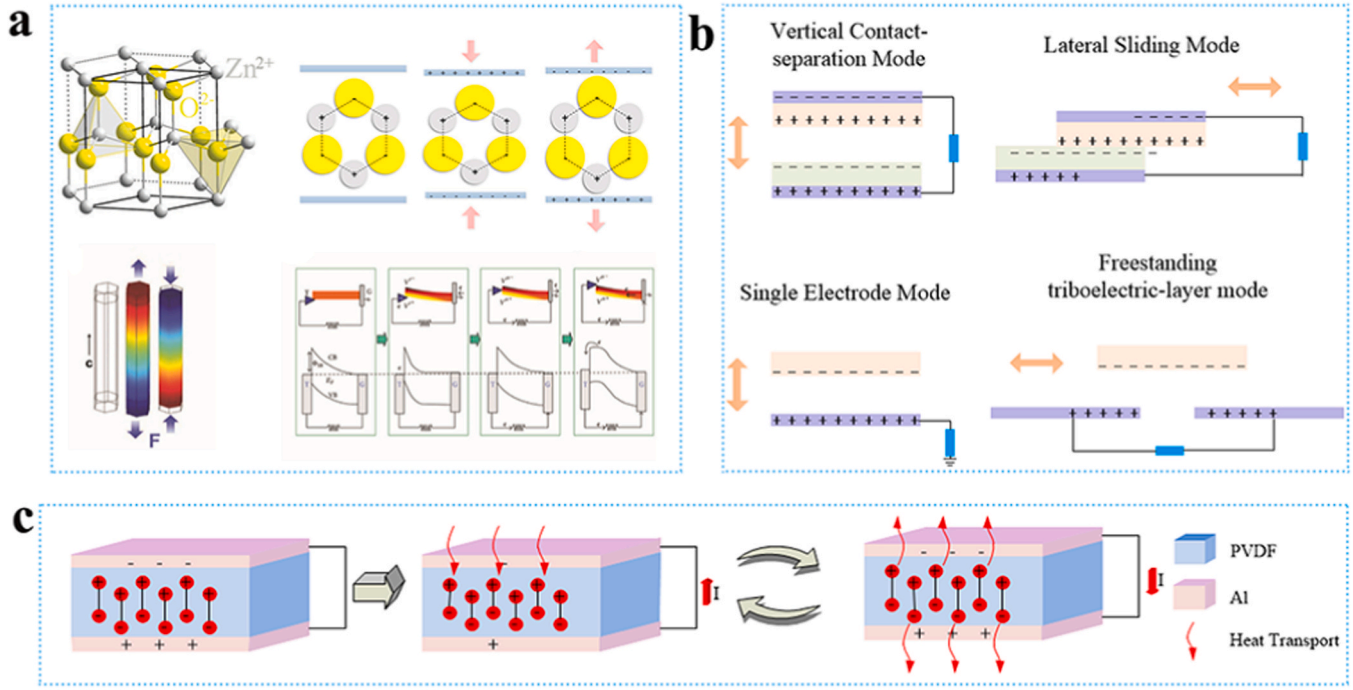

Fig. 2. (a) Mechanism of a piezoelectric nanogenerator based on a ZnO nanowire. (b) Four fundamental working modes of TENGs. (c) Schematic diagram of the working mechanism of PYENGs.
(a) Reproduced with permission [90]. Copyright 2010, Elsevier. (c) Reproduced with permission [97]. Copyright 2012, American Chemical Society.

medical applications, TENG can collect biomechanical energy from human muscle movement, heartbeat, and respiration to detect physiological signals and treat diseases [83,84]. Here we review the design and working principles of nanogenerators; summarize their applications in neuromodulation, cardiac monitoring, chemotherapy, tissue repair, artificial retinas, motion correction and training; and describe the future prospects of nanogenerators in biomedical engineering (Fig. 1).

2. Classification and working principles of nanogenerators

The theories of nanogenerators are derived from Maxwell's displacement current mechanism [85,86]. According to the principle of polarized charge generation, nanogenerators are classified as PENGs, TENGs, and pyroelectric nanogenerators (PYENGs).

2.1. PENGs

PENGs are self-powered devices that use the piezoelectric effect to collect external mechanical energy and convert it into electrical energy [87,88]. PENGs are composed of external driving electrodes, piezoelectric materials that generate piezoelectric effects, and flexible fixed substrates.

Piezoelectric materials, as the core component of PENG, realize current generation by mechanically polarizing a dielectric crystal with a certain structure. Once the piezoelectric material deforms, the internal positive and negative charge centers no longer overlap due to relative movement, leading to the generation of opposite bound charges at both ends of the material [89]. As common piezoelectric materials, ZnO, lead zirconate titanate (PZT) and polyvinylidene fluoride (PVDF), are widely used in flexible piezoelectric devices for implantable and wearable medical devices. Taking wurtzite ZnO as an example, Zn^{2+} and O^{2-} coordinate to form a tetrahedron in the ZnO crystal (Fig. 2**a**) [90]. Driven by the external force, the crystalline structure of ZnO is deformed, and the positive and negative charges are separated from the center. For ZnO nanowires, the bent structure inevitably leads to asymmetrical deformation; the inner surface of the nanowire is compressed, and the outer surface is stretched. As a result of coupling of the semiconductor and the piezoelectric properties of ZnO, negative and positive potentials are generated on the inside and outside of the nanowires, respectively. In addition, the Schottky barrier controls the flow of carriers. The generated charge is temporarily stored in the ZnO nanowire when the formed Schottky barrier is reverse biased. Once the external electrode is connected to the nanowire, the Schottky barrier is forward biased, the electrode generates an output current, and the current flows into the nanowire to generate electrical energy [91,92].

2.2. TENGs

The typical TENG has two different friction layers and one/two metal electrode. The power generation principle of TENGs is based on the coupling of the triboelectric effect and electrostatic induction effect [93–95]. The electric charge is generated and transferred at the interface of the two friction layers, and the corresponding output is generated through the electrode layer [50,96]. According to the working modes, TENGs can be divided into vertical contact-separation mode, lateral sliding mode, single-electrode mode, and freestanding triboelectric-layer mode (Fig. 2**b**).

2.2.1. Vertical contact separation mode

In vertical contact separation mode, TENG has two friction layers of different electrical polarities. Because of external pressure, the friction layers are in contact with each other, causing the friction surfaces to generate equal and opposite charges. When the external pressure gradually decreases, the two friction layers separate and an electric potential is generated between the two electrodes, driving electron flow. Once the two friction layers come into contact again, the electric potential disappears, thereby achieving electrical balance.

2.2.2. Lateral sliding mode

The device structure of the lateral sliding mode is similar to that of vertical contact separation mode. The difference is that the two friction layers of the lateral sliding model slide in the horizontal direction to realize contact and separation in the horizontal direction, thereby generating charges on the two friction layers and polarizing in the sliding direction. The electric potential drives the flow of electrons on the two electrodes and generates alternating current by periodic horizontal sliding.

2.2.3. Single electrode mode

Unlike the above two modes, the single-electrode mode has only one electrode. One end of the electrode is connected to the external circuit and the other is in contact with and separated from the triboelectric layer to generate capacitance changes. The single electrode is connected to an external reference electrode (a large conductor or ground) to exchange electrons to generate a current, and the potential reaches equilibrium.

2.2.4. Freestanding triboelectric-layer mode

The freestanding triboelectric layer mode combines the nanogenerator theory of the lateral sliding mode and the vertical contact separation mode. During movement of the independent triboelectric layer, it alternately contacts two symmetric electrodes, and an electrical potential is generated periodically to drive an alternating current through an external load. Compared with the single-electrode mode, the induced potential generated on the electrode is fully used in the freestanding triboelectric layer mode.

2.3. PYENGs

The working principle of PYENGs is based on the Seebeck effect [97], which is polarization of nanomaterials by a temperature gradient and conversion of the collected thermal energy into electrical energy (Fig. 2**c**). Nanomaterials are spontaneously polarized in the vertical direction, and the dependence of spontaneous polarization on temperature changes cause current output. When there is no temperature difference in the environment, the polarization generated by the nanomaterial is unchanged. As the temperature rises, the dipole moment and polarization density of the nanomaterial decreases, and the external circuit generates a pyroelectric current. Conversely, when the temperature of the external environment decreases, the dipole moment and polarization density of the nanomaterial increase, generating a reverse current in the external circuit. After periodic cycles, a constant pyroelectric current is generated.

3. Materials of nanogenerators

3.1. Piezoelectric materials

Piezoelectric materials are widely used in sensors and actuators. Piezoelectric materials can be divided into inorganic materials such as wurtzite semiconductor materials [98–103]; piezoelectric ceramics with high dielectric and piezoelectric properties [104–108]; and organic materials, such as PVDF and its copolymer P(VDF-TrFE) [109].

3.1.1. Inorganic materials

ZnO is a typical wurtzite semiconductor material, and ZnO nanomaterials have a high piezoelectric coefficient, low cost, and large coverage area, indicating their potential for wearable and implanted medical equipment [110]. Xue et al. reported a $0.6 \times 0.6\ cm^2$ self-powered electronic skin based on piezoelectric nanogenerators [111], which were composed of glucose oxidase-coated ZnO nanowires, Ti foil/Al foil electrodes, polydimethylsiloxane, and Kapton membranes.

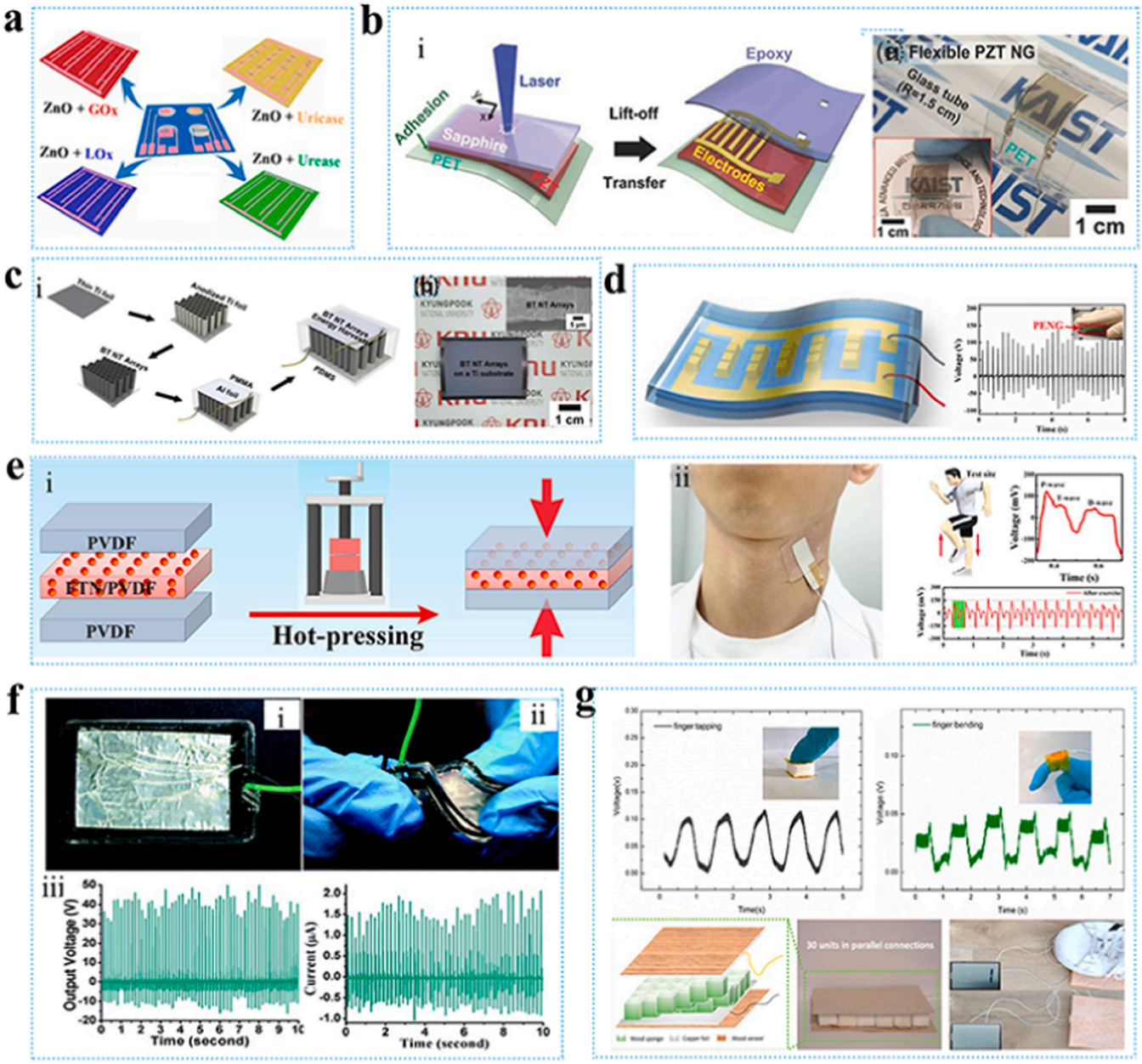

Fig. 3. Piezoelectric materials and devices. (a) A ZnO-based electronic skin for sweat analysis. (b) A high-efficiency, flexible nanogenerator composed of an ultrathin adhesive layer, a flexible substrate, and a PZT film prepared by the laser emission (LLO) method. (c) A flexible piezoelectric energy harvester (f-PEH) based on a $BaTiO_3$ nanotube array. (d) A piezoelectric nanogenerator based on P(VDF-TrFE) nanofibers and micropatterned three-dimensional (3D) interdigital electrodes. (e) A high-performance flexible piezoelectric energy harvester (FPEH) with a sandwich structure. (f) Horizontal and distorted images of a PCPENG and its electrical output when distorted. (g) When the finger presses and bends the piezoelectric nanogenerator, voltages of 0.1 and 0.06 V, respectively, are generated. Structure of a large piezoelectric nanogenerator composed of multiple wooden sponges.
(a) Reproduced with permission [113]. Copyright 2017, American Chemical Society. (b) Reproduced with permission [31]. Copyright 2014, John Wiley & Sons. (c) Reproduced with permission [105]. Copyright 2020, Elsevier. (d) Reproduced with permission [121]. Copyright 2019, Elsevier. (e, f) Reproduced with permission [122,123]. Copyright 2020, American Chemical Society. (g) Reproduced with permission [124]. Copyright 2020, American Chemical Society.

Zhang et al. used a seed-assisted hydrothermal method to vertically arrange ZnO nanowire arrays on a flexible substrate and manufactured a flexible self-powered skin implantable blood glucose meter [112]. Similarly, Han et al. developed a ZnO based piezoelectric electronic skin for perspiration analysis [113] (Fig. 3**a**). The vertically arranged ZnO nanowires (12 μm length) were prepared by a seed-assisted hydrothermal method. Four different enzymes (lactate oxidase, glucose oxidase, uricase, and urease) were modified on the surface of ZnO nanowires to form four sensing units of electronic skin. The enzyme/ZnO nanowires were cross-arranged on the interdigital electrode. For example, the lactic acid oxidase modified the sensor unit array. Reaction of lactic acid oxidase with lactic acid generated pyruvate and hydrogen peroxide; hydrogen peroxide was further decomposed to H^+, which adsorbed on the surface of ZnO nanowires under the action of an external force, resulting in a shielding effect and reducing electrical output performance. Therefore, as the concentration of lactic acid increased, the electrical output signal of the sensing unit decreased, enabling assessment of human physiology by means of electrical signals.

Piezoelectric ceramics are ceramic materials with a piezoelectric effect, typically made of several oxides and carbonates by a sintering

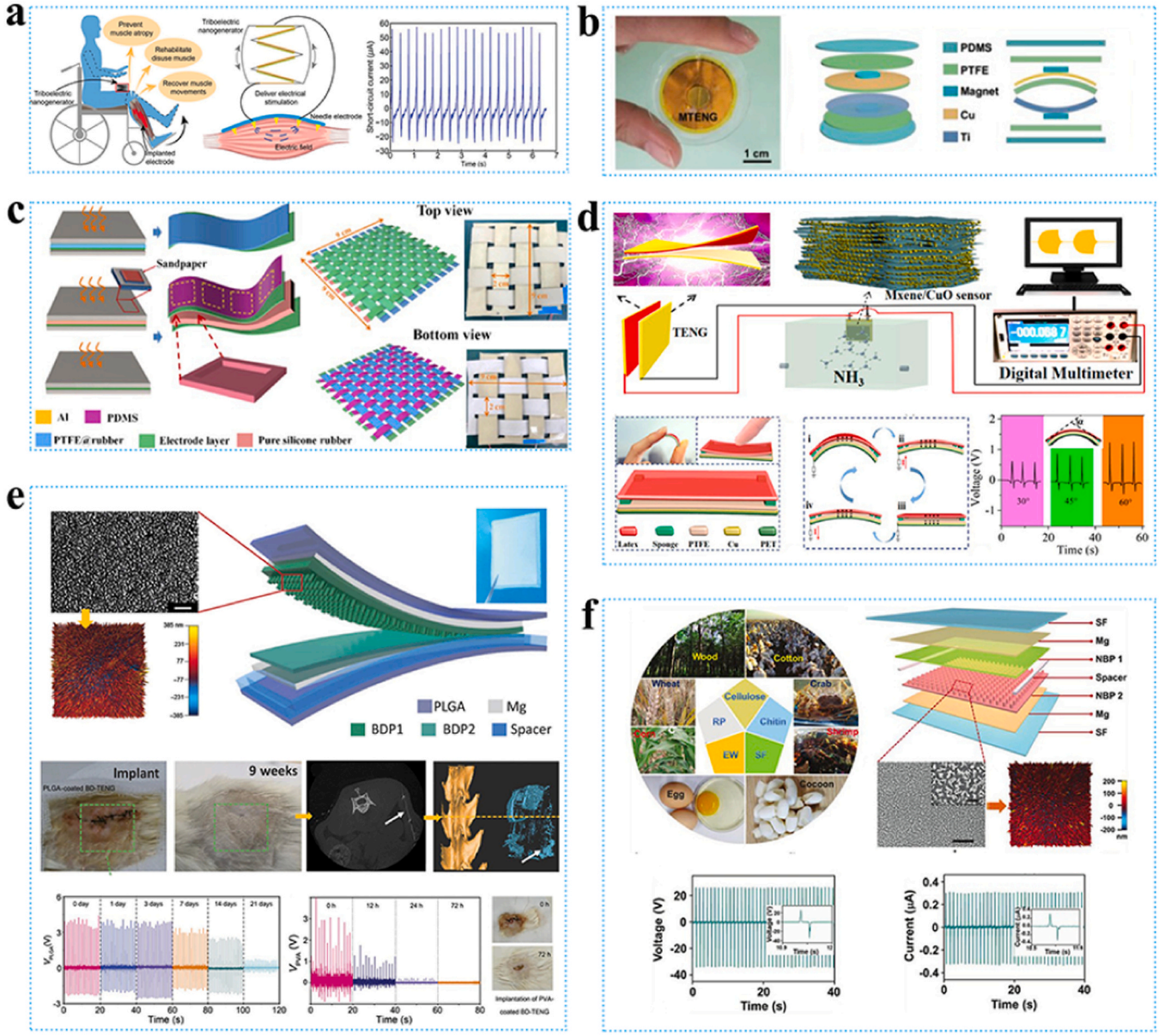

Fig. 4. Triboelectric materials and devices. (a) The TENG triboelectric layer used for muscle rehabilitation is composed of Al and PTFE. (b) The triboelectric layer of MTENG used for cancer treatment is of Ti and a nano-structured PTFE film. (c) A fully flexible HTNG with a warp-and-weft woven sandwich cavity structure. (d) A triboelectric nanogenerator based on latex and polytetrafluoroethylene. (e) BD-TENG composed of BDP1, BDP2, PLGA, Mg, and spacer. (f) The triboelectric layer material of BN-TENG is composed of SF and RP.
(a) Reproduced with permission [137]. Copyright 2019, John Wiley & Sons. (b) Reproduced with permission [138]. Copyright 2019, John Wiley & Sons. (c) Reproduced with permission [139]. Copyright 2021, Elsevier. (f) Reproduced with permission [140]. Copyright 2021, American Chemical Society.

process. Compared with piezoelectric semiconductors, piezoelectric ceramics have a higher dielectric constant and piezoelectric voltage. Piezoelectric ceramics include lead-containing and -free ceramics. Park et al. used the laser emission (LLO) method to prepare a high-efficiency, flexible nanogenerator composed of an ultra-thin adhesive layer, a flexible substrate, and a PZT film (Fig. 3**b**) [31]. The nanogenerator PZT film on a single plastic flexible substrate had high output performance. The PZT film converted mechanical energy into a ~200 V voltage and 150 μA electrical signal. Through human finger movement, the short-circuit current generated by the large-area PZT (3.5×3.5 cm^2) nanogenerator reached 8 μA, capable of driving more than 100 blue LEDs.

Although some lead-containing materials have excellent piezoelectric properties, they are harmful and have limitations for use in medical implant-mediated monitoring and treatment. Therefore, the development of lead-free piezoelectric materials is important [114]. Perovskite-type $BaTiO_3$ (BTO) is a lead-free material with excellent piezoelectric properties [115]. Jeong et al. fabricated a vertically arranged $BaTiO_3$ nanotube (BT-NT) array by electrochemical oxidation and hydrothermal reaction (Fig. 3**c**) [105]. The array had a complete perovskite crystal structure with a piezoelectric coefficient of 180 pm/v. A flexible piezoelectric energy harvester (f-PEH) based on a $BaTiO_3$ nanotube array was prepared. The f-PEH based on a single BT-NT generated a Voc of ~150 mV and a short circuit current (Isc) of ~3 nA, better than other 1D piezoelectric nanodevices.

3.1.2. *Organic polymer materials*

Although the piezoelectric coefficient of ceramics is higher than that of polymers, ceramic materials have a higher elastic modulus, hardness, and brittleness, hampering the development of flexible devices.

Compared with inorganic nanomaterials, piezoelectric polymers have extremely high flexibility; good mechanical properties, processability, and biocompatibility; and are widely used in sensors and implantable medical devices [116,117].

As a representative piezoelectric polymer, PVDF and its copolymers have been extensively studied for smart wearable devices and biomedicine because of their good flexibility, processability, biocompatibility, and chemical and mechanical stability [118,119]. Moreover, β-phase PVDF has a high dipole moment, which improves mechanical stretching and piezoelectricity [120]. Zhang et al. designed a piezoelectric nanogenerator based on P(VDF-TrFE) nanofibers [121]. Three-dimensional gold interdigital electrodes were constructed with a micropatterned quadrangular frustum pyramidal topography (micro-QFPS) (Fig. 3**d**). The polyvinylidene fluoride-trifluoroethylene copolymer P(VDF-TrFE) nanofibers were electrospun on the 3D interdigital electrodes, and the device was encapsulated in polydimethylsiloxane (PDMS). High-density micropatterns increased the output voltage of the piezoelectric nanogenerator. In a PENG with a density of 20 microstructures per electrode, the maximum output voltage and maximum power density were 50 V and 8.75 μW/cm^2 under a force of 2 kPa on an area of 1 cm^2 at 1.5 Hz, 10-fold the output performance of a planar-electrode PENG. The optimized PENG produced a maximum voltage of 150 V during finger pressing, and the rectified output drove normal operation of 32 LEDs.

Notably, the piezoelectric output performance of PVDF and its copolymer P (VDF-TrFE) is slightly lower than that of BTO and PZT, facilitating development of PVDF-based composite materials to improve output performance. Fu et al. fabricated a flexible piezoelectric energy harvester (FPEH) based on a sandwich structure, in which the middle layer was a PVDF film (2 × 2 cm^2) doped with semiconductor $FeTibO_6$ (FTN) particles, and the top and bottom layers were pure PVDF films [122]. The composite material (PVDF-FTN/PVDFx-PVDF) was produced at 200 °C and 10 MPa using a hot-pressing process (Fig. 3**e i**). The sandwich structure and doped semiconductor particles of the composite material enhanced polarization performance and electrical activity. In cantilever-beam mode, the maximum power density and charge density of P-FTN15%-P FPEH were 110 W/cm^3 and 75μ C/m^2, respectively. FPEH efficiently collected the energy generated by human movement (Fig. 3**e ii**) and bicycle movement.

3.1.3. Composite materials and natural materials

Hoque et al. used chitin nanofibers (CNF) extracted from crab shells and PVDF to fabricate a flexible and efficient piezoelectric nanogenerator (Fig. 3**f**) [123]. CNF was incorporated into PVDF to form CNF/PVDF nanocomposite material, which promoted nucleation of piezoelectric β-polymorphs. CNF/PENG (CPENG) and CNF/PVDF/PENG (PCPENG) were fabricated and their output performance was compared. At a force of 27.5 N and operating frequency of 6 Hz, the open-circuit voltage and short-circuit current generated by PCPENG were ~49 V and 1.9 μA, higher than CPENG. Moreover, PCPENG charged a 2.2 mF capacitor to 3.6 V within 20 s and drove normal operation of 22 blue LEDs.

Sun et al. fabricated a piezoelectric nanogenerator based on a wooden sponge (15 × 15 × 14 mm^3) [124]. The wooden sponge-based PENG generated an instantaneous voltage of 0.69 V and a current of 7.1 nA under a force of 13.3 kPa, which was 85-fold the electrical output performance of natural wood. The wooden sponge PENG generated a voltage output from the cyclic action of finger pressing and bending. A large-scale nanogenerator was produced by placing 30 wooden sponges connected in parallel between two pieces of copper foil and covering the copper foil with two pieces of wood veneer (Fig. 3**g**). The development of biodegradable, low-cost piezoelectric nanogenerators has overcome the disadvantages of traditional piezoelectric materials such as complex synthesis and poor ductility, providing new ideas for biomedical applications.

3.2. Triboelectric materials

Due to their different polarities, charge transfer occurs when materials contact and rub against each other. As the difference in material polarity increases, the charge transfer increases, improving the electrical output of a triboelectric nanogenerator [125,126]. Most natural materials exert a triboelectric effect, such as metals [127–130] (e.g., Al, Au, Cu, Ti) polymers [131–135] (e.g., polydimethysiloxane (PDMS)), poly-tetrafluoroethylene (PTFE), polyethylene glycol terephthalate (PET), rubber, fluorinated ethylene propylene(FEP) and degradable materials (e.g., organometallic framework, cellulose, chitin). The friction layer materials used in biomedical triboelectric nanogenerators are divided into metal-polymer, polymer-polymer, and metal-metal. Among them, metal-polymer and polymer-polymer are the mainstream friction layer materials of nanogenerators, especially for implantable medical devices.

3.2.1. Polymer-metal

The metal friction layer requires the material to have low toxicity, good biocompatibility and potential biodegradability, such as some transition metals (Mg, Zn, Fe), noble metals (Ag, Au, Pt) and non-metallic materials (Si). Wang et al. used a self-powered system to stimulate muscles that have lost function with low current to promote rehabilitation [116,136]. The TENG had a stacked structure with PET in a zigzag configuration. Al was one friction layer and electrode, and PTFE was a second friction layer, which were fixed with PET (Fig. 4**a**) [137]. TENG parallel connection improved the current output. The output power of TENG peaked at a load resistance of 5 MΩ, and the short-circuit output current was 75 μA. A disabled muscle was stimulated by a low current generated by a TENG connected to a penetrating electrode. Zhao et al. reported an implantable magnetic nanofriction generator (MTENG) for the treatment of cancer *in vivo* [138]. The nano-structured PTFE film was one of the friction layers; Au deposited on the back of the PTFE served as an electrode and Ti served as a second friction layer and an electrode (Fig. 4**b**). The magnet was adsorbed on the back of the electrode, and the contact layers were separated by a repulsive force, thereby improving the long-term output of the TENG.

3.2.2. Polymer-polymer

Polyimide (Kapton), PET, PDMS, polypropylene, are common polymer friction layers of TENGs. In recent years, biodegradable polymers, such as poly (L-lactide-co-glycolide) (PLGA), polylactic acid (PLA), chitosan, have received increasing attention in the application of implantable medical devices. Wang et al. used a flat vulcanization process to manufacture a fully flexible homogeneous integrated textile TNG (HTNG), which was woven by warp and weft [139]. The warp was a sandwich structure of an electrode layer and pure rubber layer, and each warp had four cavity structures. The wefts were woven by PTFE@rubber/electrode layer (Fig. 4**c**). The HTNG exerted an internal triboelectric effect, interlayer triboelectric effect, and external triboelectric effect. For the internal triboelectric effect, Ag@rubber served as the electrode layer and the positive friction layer, and pure rubber served as the negative friction layer. For the interlayer triboelectric effect, the PTFE@rubber weft tape and Ag@rubber warp tape were used as the friction layers. An external triboelectric effect was generated when the external Al tape contacted the HTNG. The Al tape served as the positive triboelectric layer, and PTFE@rubber and PDMS were used as the negative triboelectric layer. The mixed triboelectric effect mode showed the best point output performance with a maximum open-circuit voltage of 728 V and short-circuit current of 16.6 μA. This device makes full use of the triboelectric effect. Wang et al. reported a triboelectric nanogenerator based on latex and polytetrafluoroethylene [140]. The TENG, composed of Cu electrodes, a friction layer of latex and polytetrafluoroethylene (PTFE), and a protective layer of polyethylene (PET), drove an ammonia sensor (Fig. 4**d**). At an operating frequency of 10 Hz, the maximum peak-to-peak open circuit voltage (Voc) produced

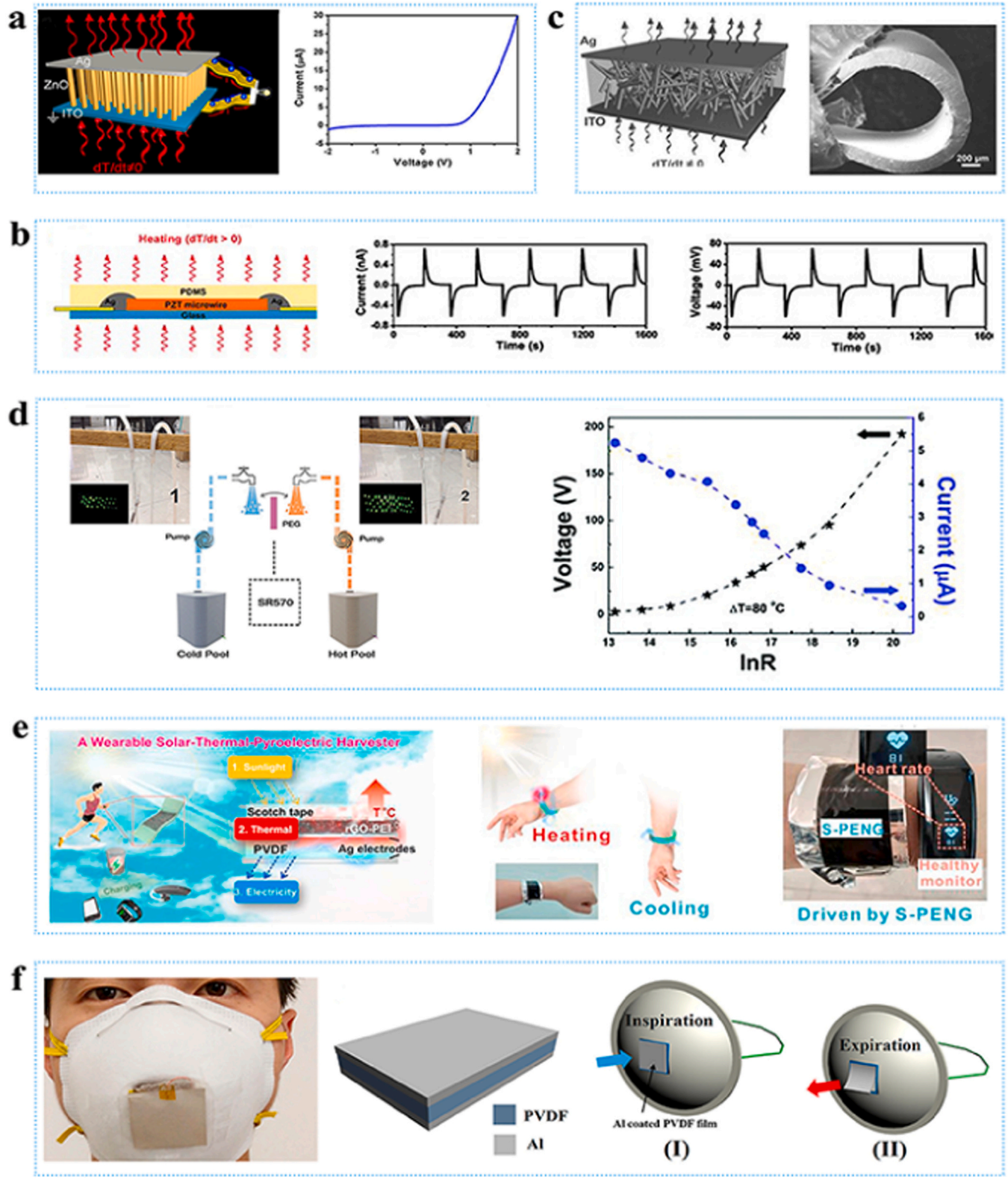

Fig. 5. Pyroelectric materials and devices. (a) Schematic diagram of the structure of ZnO-based PYENG and the I-V characteristic curve of PYENG. (b) The structure diagram of PZT-based pyroelectric nanogenerator, and the voltage and current output by PYNG. (c) The structure diagram of the $KNbO_3$-based pyroelectric nanogenerator and the SEM image of the $KNbO_3$-PDMS composite film when it is bent. (d) The PYENG-based experimental system and the output current, voltage and power of PYENG under a temperature change of 80 °C. (e) The design scheme and working principle of S-PYNG, when S-PYNG is used as a wearable device. (f) Masks based on PYENG. The structural composition of the pyroelectric nanogenerator and the schematic diagram of the respiration-driven PYENG.
(a) Reproduced with permission [152]. Copyright 2012, American Chemical Society. (b) Reproduced with permission [153]. Copyright 2012 American Chemical Society. (c) Reproduced with permission [154]. Copyright 2012, WILEY-VCH Verlag GmbH & Co. KGaA, Weinheim. (d) Reproduced with permission [150]. Copyright 2014, The Royal Society of Chemistry. (e) Reproduced with permission [155]. Copyright 2020, Elsevier. (f) Reproduced with permission [156]. Copyright 2020, Elsevier.

by the TENG was 810 V, the maximum short-circuit current was 34 μA, and the maximum power density was 10.84 W/m^2. Based on the ductility and flexibility of latex and PTFE, a triboelectric nanogenerator (3 × 2 cm^2) with a single electrode working mode was designed. This triboelectric nanogenerator used four 2-mm-thick insulating sponges to separate the latex friction layer from the PTFE layer. As the degree of bending increased, the contact area of the friction layer increased, and the voltage output signal gradually enhanced. The single-electrode mode triboelectric nanogenerator could detect human movement and respiration. In addition to selecting the optimum friction-layer material, the structure can be optimized to improve the stability and durability of TENG. Yu et al. fabricated an implantable piezoelectric nanogenerator composed of a mesoporous PVDF film (1 × 2 × 30 μm^3). Mesoporous PVDF improved the flexibility of the material [119]. Moreover, the different thickness of PDMS increased the tension and compression portion of dipoles, enhancing the electrical performance of the piezoelectric nanogenerator.

Biodegradable and absorbable materials are essential for implantable medical devices for short-term treatment. There is no need to perform surgery to remove the equipment after completion of treatment, reducing the cost and surgical risk [141,142]. Zheng et al. fabricated a biodegradable triboelectric nanogenerator (BD-TENG), which could be degraded and absorbed after energy conversion was completed [143]. The biodegradable polymer (BDP) layer can be PLGA, poly (3-hydroxybutyric acid-co-3-hydroxyvaleric acid) (PHB/V), poly (caprolactone) (PCL), or poly (vinyl alcohol) (PVA). The BDP materials were used as friction parts, spacers, and encapsulated layers. The Mg electrode was also biodegradable (Fig. 4**e**). After 9 weeks of implantation in rats, PLGA-coated BD-TENG had an incomplete structure, and the BD-TENG materials were degraded. PVA-coated BD-TENGs functioned for more than 24 h in rats with a maximum output voltage of ~3 V. The voltage output dropped to 0 within 72 h, indicating that the PVA-coated BD-TENGs were completely dissolved. Jiang et al. designed a degradable triboelectric nanogenerator based on bioresorbable natural polymers (BN-TENG) [144]. The friction layer material could be cellulose, chitin, silk fibroin (SF), rice paper (RP), or egg white (EW) (Fig. 4**f**). When SF and RP were used as friction layers, the maximum output open-circuit voltage and short-circuit current of BN-TENG were 34 V and 0.32 μA, respectively. The electrical output signals of the forward and reverse connections were identical, and current output was positively correlated with external load. The maximum power density was 21.6 mW/m^2 at an external load of ~67 Ω. The BN-TENG was completely degraded and absorbed in SD rats.

3.3. Pyroelectric materials

The thermoelectric energy required by the pyroelectric material is obtained through the Seebeck effect, and the temperature difference between the two ends of the device drives the flow of carriers. Anisotropic materials change in temperature with time, which causes spontaneous polarization of the material, and converts thermal energy into electrical energy [145,146]. The performance of pyroelectric nanogenerators has been improved through the application of different pyroelectric materials. Pyroelectric materials widely used in pyroelectric nanogenerators mainly include ceramics (ZnO, PZT, and lead-free ceramics) and polymers (PVDF, P(VDF-TrFE)) [147–151].

3.3.1. Ceramic-based pyroelectric nanogenerators

Zhong-Lin Wang's group reported a thermoelectric nanogenerator based on ZnO pyroelectric nanowire arrays (Fig. 5**a**). ZnO nanowires were grown on an indium tin oxide (ITO) substrate by solution growth technology, with ITO as the bottom electrode. The Ag film deposited on the ZnO served as the top electrode while forming Schottky contact with ZnO [152]. As the temperature increased and decreased, the thermoelectric potential was generated and disappeared in the ZnO nanowires, allowing electrons to flow in the external circuit. The peak output voltage and current of PYENG were 5.8 mV and 108 pA, respectively. Meanwhile, the output performance of PYENG increased as the temperature change rate increased. They also developed a PZT Micro/Nano wire based PYENG for detecting temperature change (Fig. 5**b**). The PYENG was composed of a single PZT nanowire (10 μm in length, 2 μm in diameter). The PZT Micro/Nanowire was placed on a thin glass substrate and packaged in PDMS [153]. The peak output voltage and current of PYENG were 60 mV and 0.6 nA, when the temperature changed from 296 K to 333 K. As the output voltage of PYENG increased linearly with the increase of the temperature change rate, PYENG could be used as a sensor to measure the surface temperature of the contacting heat source. Based on the above principles, the authors measured the temperature of the finger surface (303 K) and lighted a LCD at a high temperature of 473 K. The non-toxic properties of lead-free pyroelectric materials are of great significance to the development of PYENG in biomedical and wearable devices. Wang's group used single crystal lead-free $KNbO_3$ nanowires to fabricate PYENG [154]. PDMS and $KNbO_3$ nanowires were mixed in a volume ratio of 7:3, which effectively improved the flexibility of PYENG (Fig. 5**c**). ITO was used as the bottom electrode and silver was used as the top electrode. When the temperature change rate was 2 K s^{-1}, the peak output voltage of PYNG was 10 mV and the current was 120 pA.

3.3.2. Polymer-based pyroelectric nanogenerator

Recently, some polymers have been used in PYENGs due to their promising pyroelectric properties. Waste water from industrial production and household life contains a lot of waste heat, which is a huge energy source. Xi and Hu group developed a PYENG based on PVDF film [150], which could collect thermal energy from water. The cold and hot water were respectively transported to the upper side by the pump, and the PYENG moved back and forth under the action of the oscillator, so as to achieve alternate contact with the cold and hot water, and generated electrical signals when it contacts the fluid. When the temperature rose from 40 °C to 80 °C, the maximum open circuit voltage reached 192.6 V, the short circuit current was 12 μA/cm^2, and the output power density was 14 μW/cm^2. PYENG could charge a 100 μF capacitor to 3.3 V and light up the LED (Fig. 5**d**). Li et al. reported a sunlight triggered pyroelectric nanogenerator (S-PYNG) (Fig. 5**e**). The pyroelectric film, as a key structure to improve the efficiency of pyroelectrics, was composed of polyethyleneimine (PEI) reduced graphene oxide (rGO-PEI) and polarized polyvinylidene fluoride (PVDF) film [155]. The output power of S-PYNG could reach 21.3 mW/m^2. A bracelet made of S-PYNG (3 × 9 cm^2) was worn on the wrist and exposed to sunlight. By waving hand to create temperature gradient, the SPYNG output current could reach 120 nA. Xue et al. produced a wearable PYENG based on N95 respirator and polyvinylidene fluoride (PVDF) film to collect the heat generated by human respiration (Fig. 5**f**). When the temperature change range of the gas exhaled by the human body was 5 °C, the peak open circuit voltage of PYENG was 42 V, and short circuit current produced by PYENG was 2.5 μA. When the external load was 50 MΩ, the maximum power reached 8.31 μW. PYENG could charge the capacitor to 1 V within 18 s, and successfully lighted up the LCD and LED [156].

Currently, PYENGs have been used in some wearable equipment, such as bracelets, masks, etc. However, there are few reports on their application in biomedical sensing and treatment. Therefore, the biological applications introduced below mainly focus on TENGs and PENGs. It can be expected that PYENGs will have broader application prospects in the field of breathing and body temperature detection in the future.

4. Biomedical applications

4.1. Modulation of neural activity and the construction of brain-electric interface

The nervous system plays an important role in the reception and

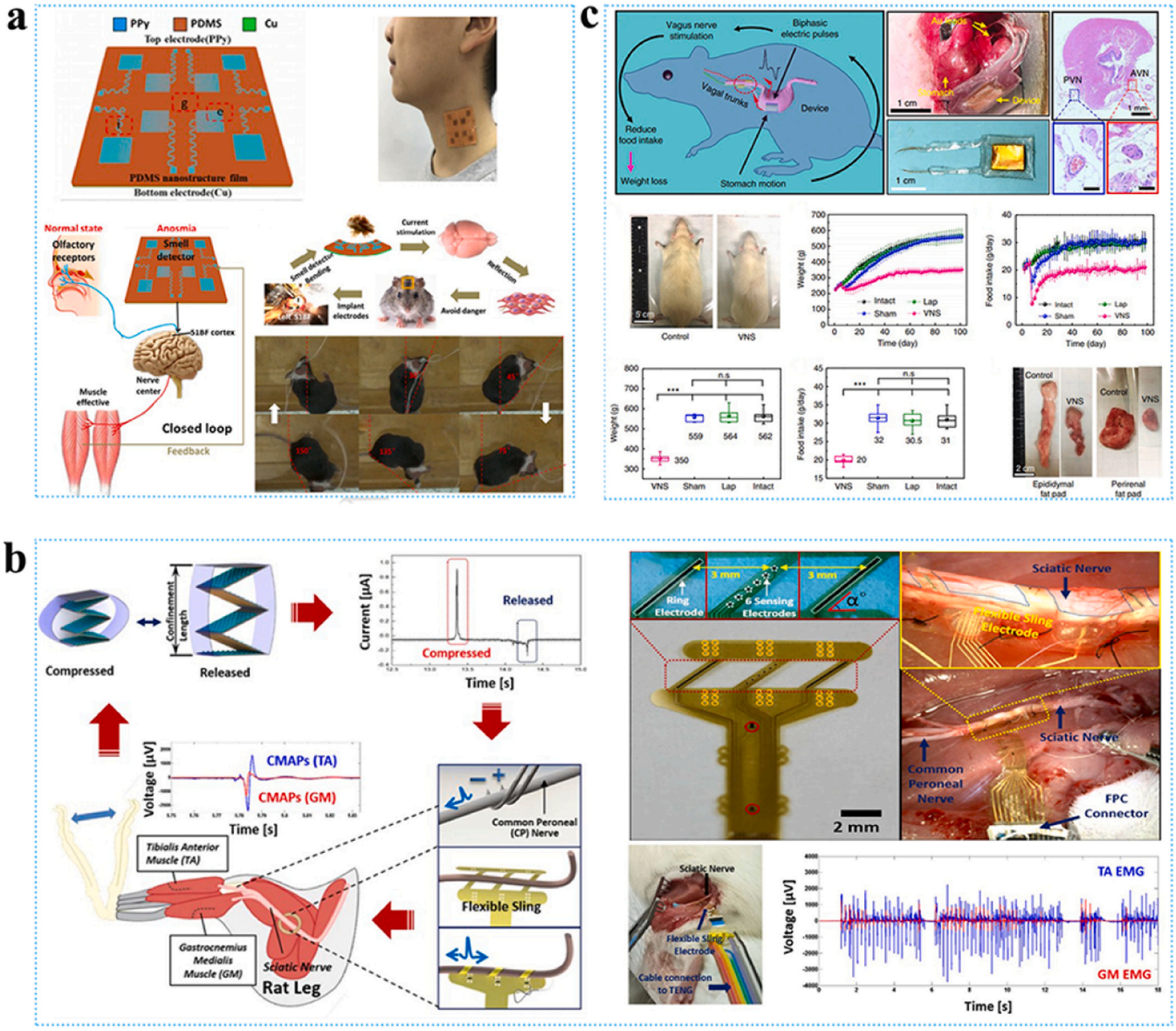

Fig. 6. Nanogenerators for neuromodulation. (a) A flexible electronic olfactory sensor constructed based on a triboelectricity-brain-behavior closed loop. (b) Foldable TENG that can selectively activate muscles through a neural interface. (c) TENG implanted in the stomach of rat to control body weight by stimulating the vagus nerve.

(a) Reproduced with permission [157]. Copyright 2019, Elsevier. (b) Reproduced with permission [160]. Copyright 2017, Elsevier. (c) Reproduced according to the terms of the CC-BY license [161].

transmission of physiological signals in various parts of the human body. In the clinic, the signals generated by the nervous system are essential for the diagnosis and treatment of diseases. Nanogenerators, which have excellent electrical performance, provide an external source of power for nerve stimulation. The pulse current stimulates innervating motor nerve fibers, afferent sensory nerve fibers, and promotes the plasticity of the human brain, thereby regulating physiological functions.

Nanogenerators can be integrated with sensors, and realize the simulation of smell and taste through the connection with the brain. Zhong et al. constructed a triboelectricity-brain-behavior closed loop and fabricated a flexible electronic olfactory sensor [157]. The olfactory detection device had eight sensing units with dimensions of 0.6×0.6 cm^2. The friction layers of the sensing unit were composed of polydimethylsiloxane/polypyrrole (PDMS/PPy). The PPy structure of each sensing unit was doped with different dopants or surfactants. Volatile chemicals in the environment react with specific PPy derivatives, thereby affecting the surface state of PPy and producing different output currents, enabling the identification of specific gases. The olfactory detector was connected to the brain to trigger a certain behavior, forming a closed-loop behavior-triboelectricity-brain behavior system (Fig. 6**a**). Stimulating the left primary somatosensory cortex caused the mouse to turn right, simulating avoidance of a toxic atmosphere. Zeng et al. proposed a triboelectric biosensing electronic skin that is also based on polydimethylsiloxane/polypyrrole (PDMS/PPy) [158]. This electronic skin could be used to detect the pH and alcohol content of beverages and can effectively simulate an artificial taste system. When the electronic skin was connected to the primary motor cortex of the rat's brain, the electrical signals generated by the electronic skin can act on the rat's perception and promote the movement of the rat's legs, thereby realizing behavioral intervention.

Electrical stimulation can act on the reflex arc knot structure to activate muscle movement. Hwang et al. developed a flexible energy harvester based on indium-modified crystalline $Pb(In_{1/2}Nb_{1/2})O_3$–$Pb(Mg_{1/3}Nb_{2/3})O_3$–$PbTiO_3$ (PIMNT) film, which converted mechanical

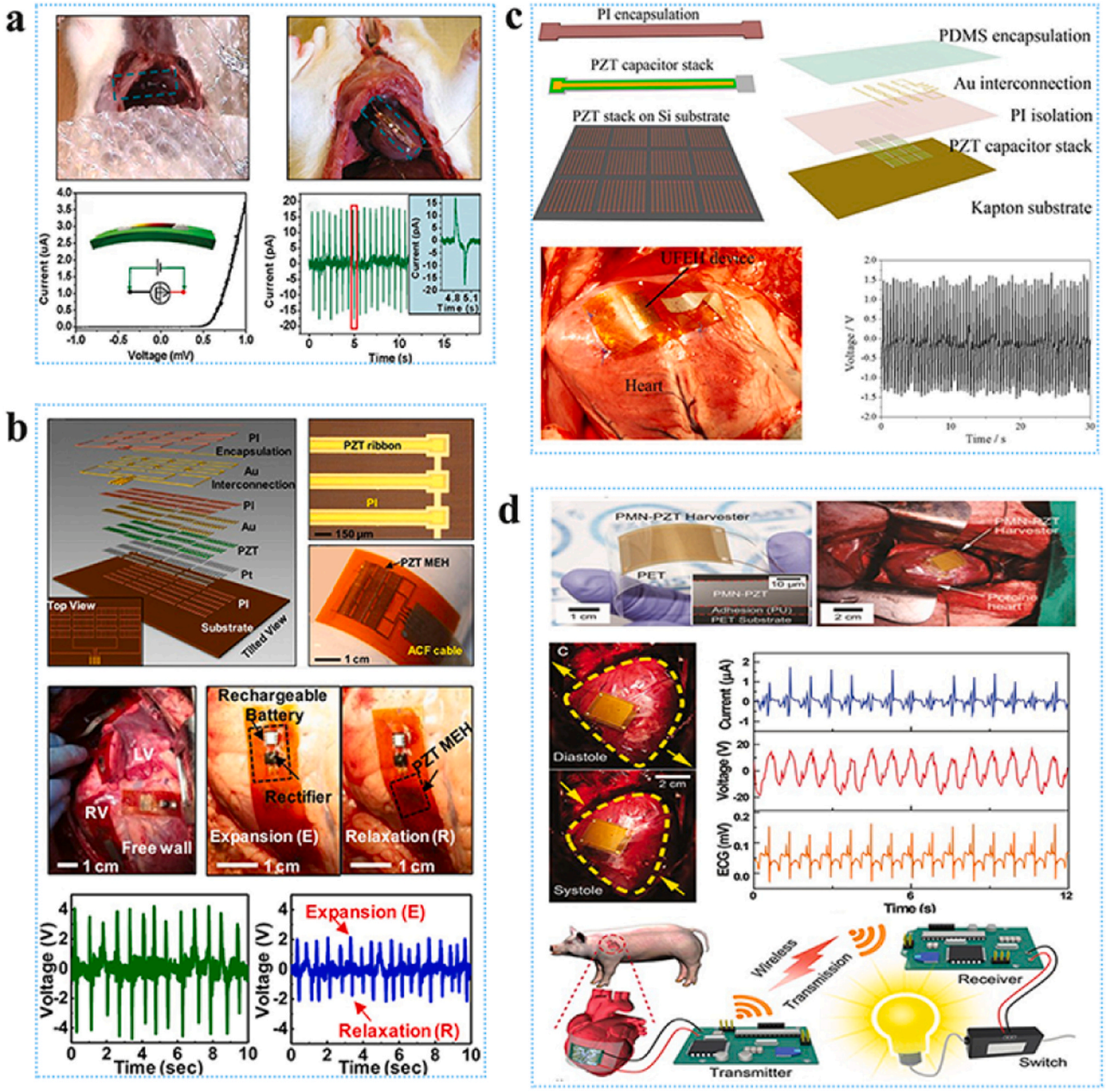

Fig. 7. Piezoelectric nanogenerators implanted in the hearts of animals. (a) SWG implanted into rat diaphragm and heart to generate electrical current for biomechanics of respiration and heartbeat. (b) Integrated PZT MEH system implanted into the right ventricle, left ventricle, and free wall of an animal heart to collect, store, and convert energy from the heartbeat. (c) UFEH implanted into animal hearts to collect and transform biomechanical energy, and to supply energy to commercially available pacemakers. (d) Piezoelectric nanogenerator implanted between the right ventricle and the apex of the left ventricle to record the ECG signal. (a) Reproduced with permission [163]. Copyright 2010, John Wiley & Sons. (b) Reproduced with permission [164]. Copyright 2014, National Academy of Sciences of the United States of America. (c) Reproduced according to the terms of the CC-BY license [165]. (d) Reproduced with permission [166]. Copyright 2017, John Wiley & Sons.

motion into electricity for deep-brain stimulation (DBS) [159]. The single crystal PIMNT film improved the output electrical signal with a maximum output current of 0.57 mA, achieving the threshold current for real-time DBS of the motor cortex. The PIMNT-based nanogenerator was connected to the stimulation electrode and transmitted electricity to the M1 cortex of the mouse brain, successfully inducing movement of the forearm. Captured video showed that when the device was bent, the right paw of the mouse moved 1.5–2.3 mm under electrical stimulation. Lee et al. designed a foldable TENG with a stacked structure as a nerve stimulation power source, which could be connected to a nerve interface to stimulate the sciatic nerve and common peroneal nerve and selectively activate muscles [160]. The PET substrate was folded into a zigzag shape to fit the stacked design, providing the restoring force between the friction layers in the compressed state. The electrical signals were transmitted to the common peroneal (CP) nerve through the neural interface, activating the tibialis anterior (TA) muscle. The compound muscle action potential (CMAP) indicated that the TA muscle is more easily activated than the GM muscle (Fig. 6**b**). The results indicated that the TENGs with a neural interface will be useful for implantable battery-less neuromodulators.

Nanogenerators can also regulate organ functions through electrical signals. Yao et al. fabricated a device to stimulate the vagus nerve (VNS) based on an implantable and flexible TENG [161]. TENG was implanted on the surface of a rat stomach to convert the mechanical energy of

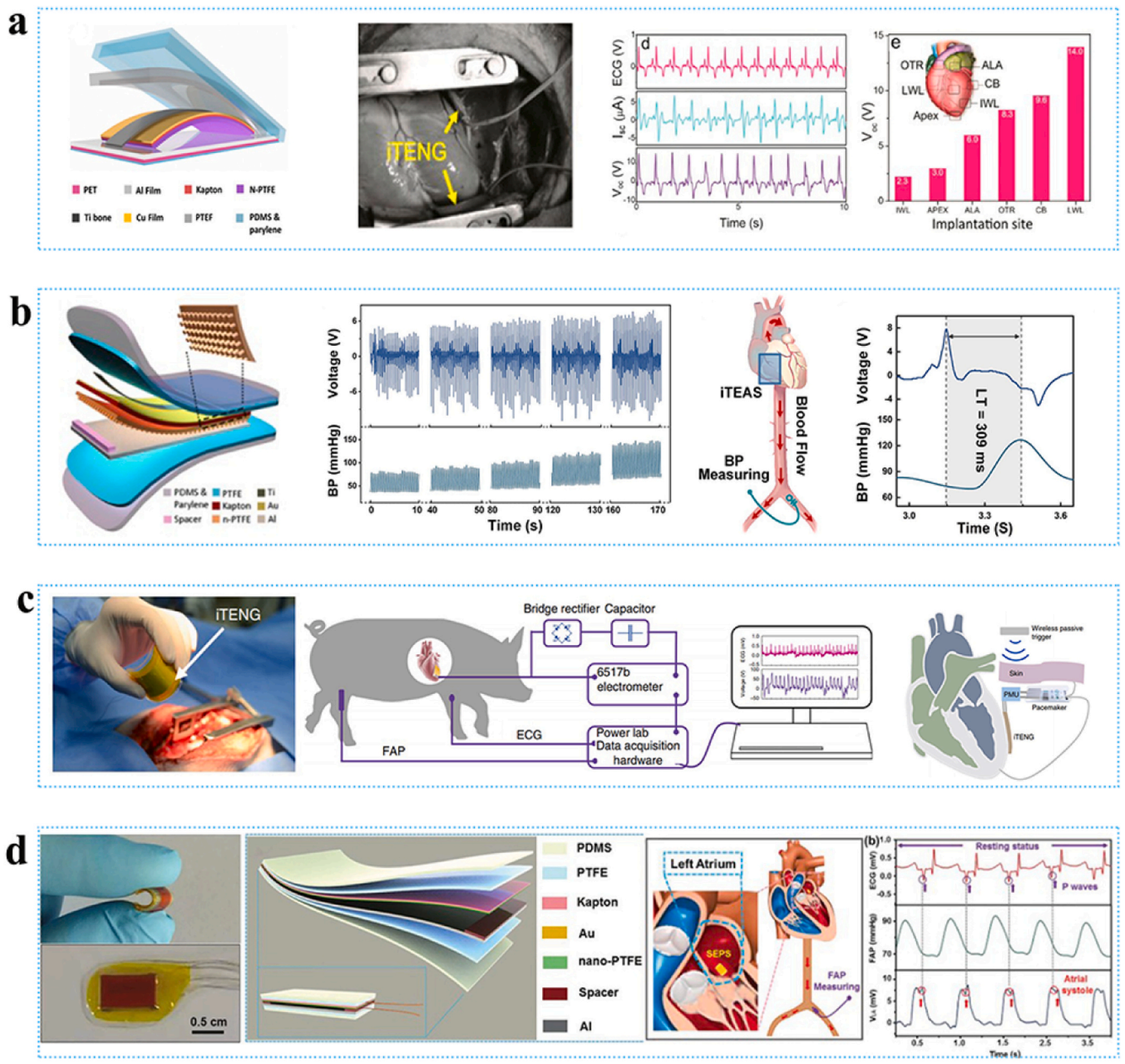

Fig. 8. Triboelectric nanogenerators implanted in animal hearts. (a) iTENG implanted between the heart and pericardium of a pig to record the ECG signal. (b) Blood pressure measurement by iTEAS. (c) *In vivo* collection and transformation of the mechanical energy generated by heart movement to drive a cardiac pacemaker. (d) SEPS implanted into the left atrium to measure FAP and ECG signals by means of a pressure sensor attached to the right femoral artery.
(a) Reproduced with permission [168]. Copyright 2016, American Chemical Society. (b) Reproduced with permission [169]. Copyright 2016, American Chemical Society. (c) Reproduced according to the terms of the CC-BY license [171]. (d) Reproduced with permission [172]. Copyright 2019, John Wiley & Sons.

gastric contraction and relaxation into electrical signals, and stimulated the vagus nerve, reducing food intake and achieving weight control (Fig. 6**c**). Compared with the control rats, VNS rats achieved 35% weight loss within 18 days, and maintained a weight loss of 38% during the remaining test period (75 days). After 100 days of weight control, the average weight of the epididymal and perirenal fat pads were 58% and 67%, respectively, lower than the control. The weight of rats was reduced by 38% compared with the controls. In addition to controlling gastric function, foldable triboelectric nanogenerators can be used to stimulate bladder nerves and regulate bladder function [162]. Pelvic nerves are stimulated by multiple pulses to contract the bladder and initiate urination. Therefore, the nanogenerator-based neurostimulation system has potential for regulating and improving bladder function.

4.2. *Diagnostic monitoring and treatment of the cardiovascular system*

It is necessary to detect the physiological and pathological signals of patients with cardiovascular diseases, such as heart rate, blood pressure, and ECG parameters. Nanogenerators convert biomechanical energy into electricity and monitor small changes in physiological and pathological indicators. Moreover, electrical stimulation by the nanogenerator can be used to drive a pacemaker and improve the function of myocardial cells.

4.2.1. *Implantation of a nanogenerator into the heart*

Early research on nanogenerator in the field of cardiovascular applications mainly focused on PENG. In 2010, Li et al. used ZnO-based

alternating current and single-wire nanogenerators (SWG) to collect energy from rat respiration and heartbeat of rat for the first time (Fig. 7**a**) [163]. The SWG was implanted on the surface of the heart, and the Voc and Isc increased to 3 mV and 30 pA, respectively. In 2014, Dagdeviren et al. developed arched PZT piezoelectric devices (MEH) for energy collection and storage from the contraction and relaxation of the heart, lungs, and diaphragm (Fig. 7**b**) [164]. The flexible PZT piezoelectric energy harvester comprised Ti/Pt and Cr/Au electrodes with a PZT layer sandwiched between the electrodes. Cardiac parameters such as size, heart rate, and contractility affected voltage output. Due to the distinct heart structures between different species, for example, the mass of bovine heart is almost twofold that of ovine heart, so the output voltage of PZT MEH in the bovine model was higher than in the sheep model. Pacemakers and dobutamine injections also affect the output voltage of PZT MEH. The device exceeded 20 million bending/extension cycles in a humid hydrogel environment, revealing that the flexible PZT-MEH is stable in vivo.

Lu et al. implanted an ultra-flexible PZT piezoelectric device (UFEH) into an animal heart to collect mechanical energy to drive a pacemaker continuously (Fig. 7**c**) [165]. The UFEH was fabricated by photolithography and transfer-printing technology. The main structure of the flexible piezoelectric device was a PZT-based nanocapacitor, with Pt and Au as the bottom and top electrodes, respectively. The PI-coated PZT wafer was fixed on a silica substrate by photolithography and wet etching to form a PZT nanoribbon array. The UFEH was sutured to the outer membrane of a pig heart. Like the Dacron patch used in cardiac surgery, the flexible energy harvester did not affect normal physiological activities. The UFEH was implanted into the anterior wall of the apex, and the peak-to-peak output voltage was 3 V. Therefore, UFEH can use the biomechanical energy generated by heart movement and has potential an implantable power source for cardiac pacemakers.

Kim et al. used high-performance single crystal PMN-PZT in a flexible bioenergy harvesting device with self-powered wireless transmission [166]. The Mn-doped PMN-PZT had a high pressure-point charge coefficient and electromechanical coupling coefficient ($d_{33} \approx 1140$/PCN, $K_{33} \approx 0.92$). To demonstrate energy collection in vivo, the energy-harvesting device was fixed between the right ventricle and the apex of the left ventricle of Yorkshire pigs. As the heart contracted and relaxed, piezoelectric energy harvester was bent and released. The measured Voc and Isc were 17.8 V and 1.75 μA, respectively, and the pig ECG signal was recorded simultaneously. The collection device converted biomechanical energy into electrical energy and functioned simultaneously with a radio communication device in vivo. Energy from heart movement was stored in a capacitor via a full-wave bridge rectifier and wirelessly transmitted to the receiver, controlling repeated activation/deactivation of a bulb (Fig. 7**d**).

Due to its universal applicability and high efficiency, TENG is increasingly used to collect the mechanical energy of living organisms [167]. In particular, biodegradable TENG is gradually being used for cardiac monitoring and treatment. Zheng et al. developed an

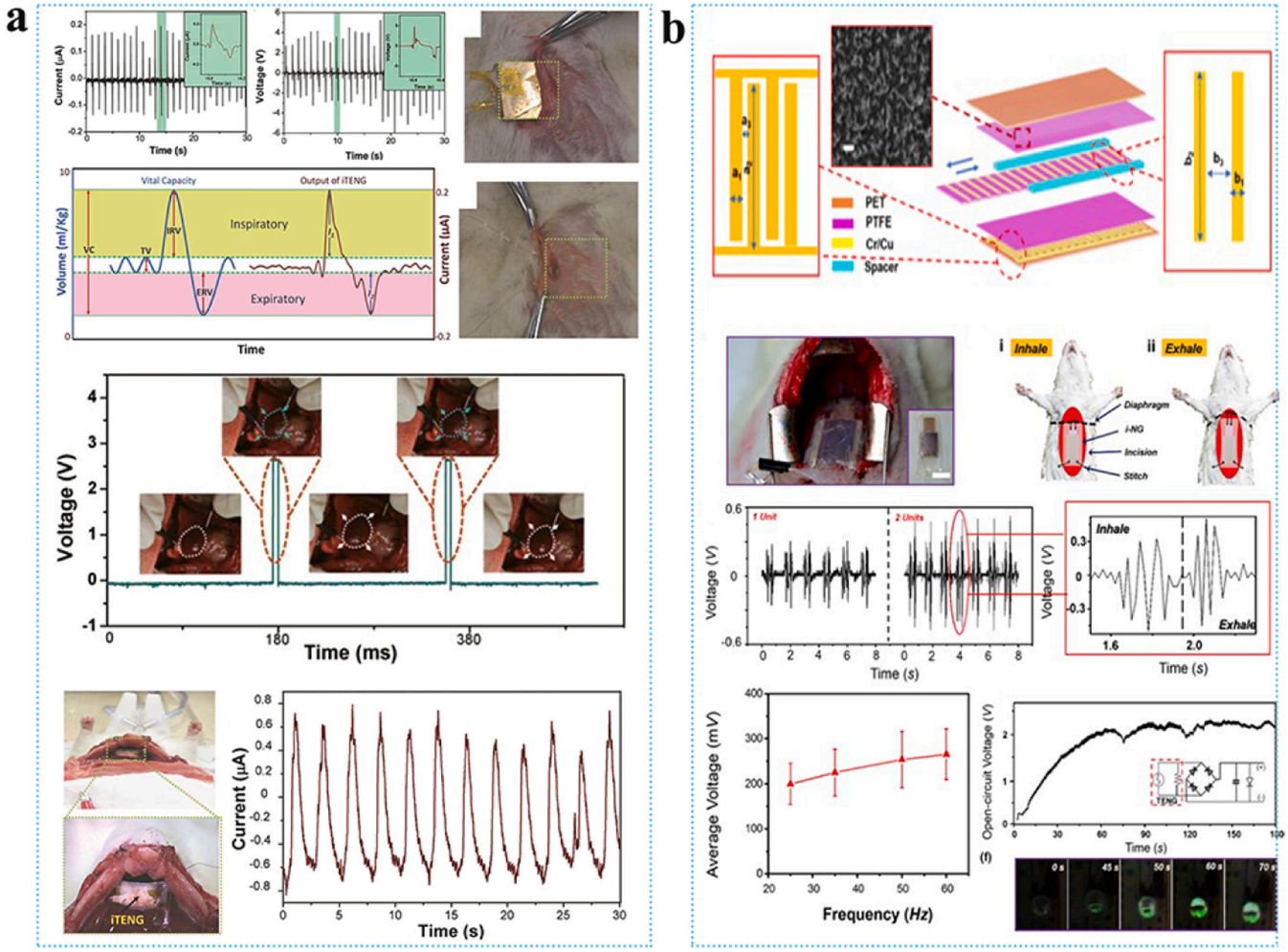

Fig. 9. Nanogenerators implanted into the thoracic and abdominal cavities. (a) iTENG implanted under the skin of the thoracic cavity of a living rat, to collect energy from respiration to drive a pacemaker. (b) i-NG implanted into the abdominal cavity of SD rat to collect the biomechanical energy of respiration.
(a) Reproduced with permission [173]. Copyright 2014, John Wiley & Sons. (b) Reproduced with permission [174]. Copyright 2018, American Chemical Society.

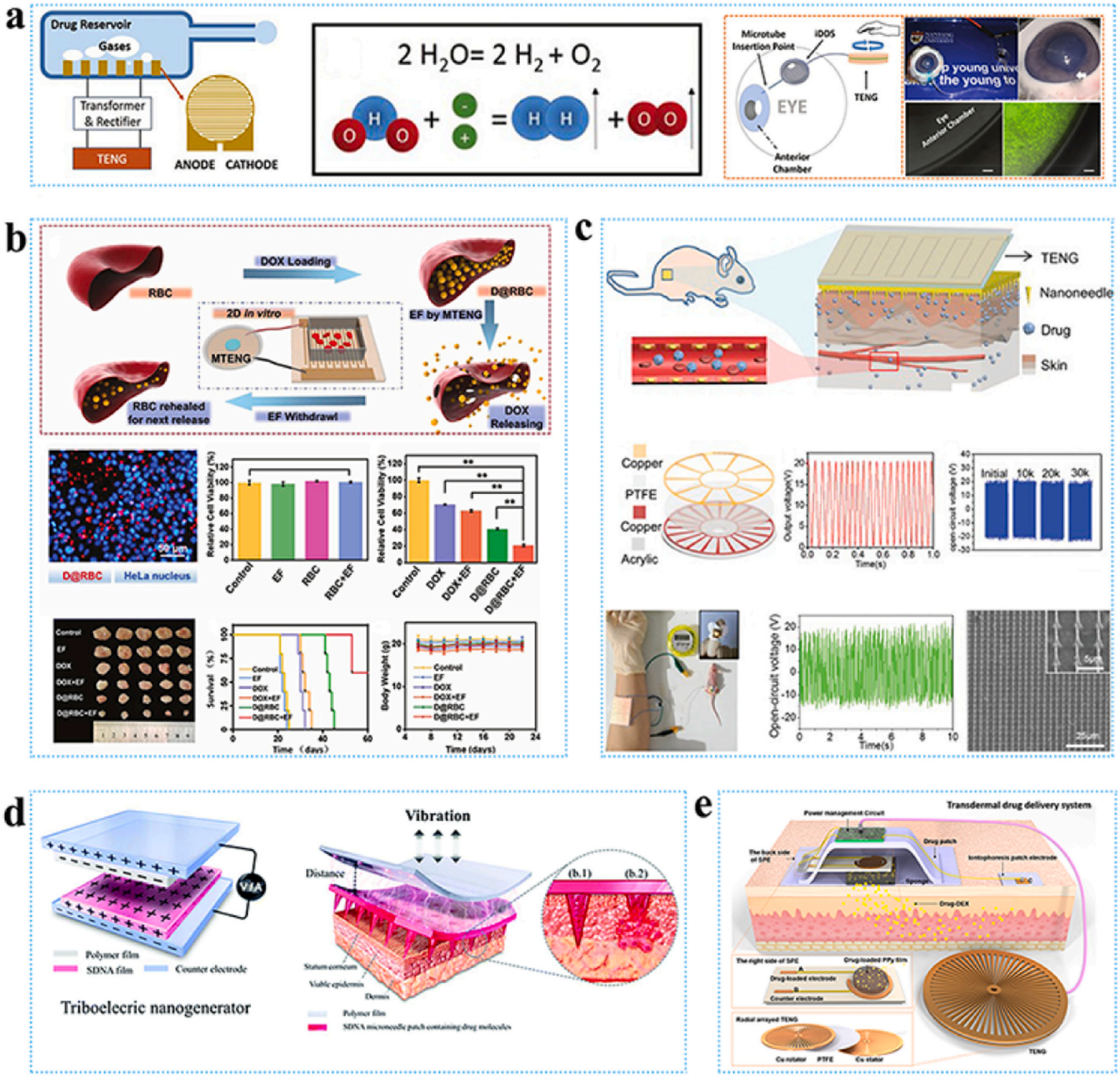

Fig. 10. Drug delivery system based on a nanogenerator. (a) *In vitro*, transscleral drug delivery based on an iDDs system in pig eye. (b) Cancer treatment based on a DDS system controlled by MTENG. (c) Drug pumping by in vitro and *in vivo* electroporation systems. (d) TENG based on SDNA membrane and polymer layer, and a drug delivery system coupled with SDNA microneedles and TENG. (e) TENG-driven self-powered transdermal drug delivery system delivers on-demand and precise drug delivery.

(a) Reproduced with permission [175]. Copyright 2017, John Wiley & Sons. (b) Reproduced with permission [176]. Copyright 2019, John Wiley & Sons. (c) Reproduced with permission [177]. Copyright 2019, John Wiley & Sons. (d) Reproduced with permission [178]. Copyright 2018, Royal Society of Chemistry. (e) Reproduced with permission [179]. Copyright 2019, Elsevier.

implantable friction nanogenerator (iTENG) for powering implantable medical devices and self-powered wireless cardiac monitoring *in vivo* [168]. iTENG was composed of an encapsulation layer, a 'keel structure' friction layer, and an electrode layer. The friction layer contained nano-structured polytetrafluoroethylene. The Kapton film was used as a flexible substrate, and a 50 nm Au layer was deposited on the back of the Kapton film to form an electrode. Aluminum foil was the other electrode and the friction layer. Highly elastic titanium served as a keel structure to control contact and separation of the friction layer (Fig. 8**a**). The iTENG was implanted between the heart and the pericardium of a Yorkshire pig, and the friction layer contacted and separated under periodic cardiac contraction and relaxation. The Voc of iTENG reached ~14 V, and the short-circuit current was 5 μA. The output performance of the iTENG was greatest in the lateral wall of the left ventricle, and the Voc was 14 V. The iTENG was implanted between the heart and pericardium showed a stable output signal and enabled normal cardiac function in the long-term.

Ma et al. developed a self-powered, one-stop, multifunctional implantable triboelectric active sensor (iTEAS) for real-time biomedical monitoring [169] (Fig. 8**b**). The iTEAS, which had dimensions of $30 \times 20 \times 1$ mm^3, was composed of a triboelectric layer, electrode, spacer layer, and encapsulation layer. The friction layers were of

aluminum and PTFE (50 μm); nano-structured PTFE was fixed on the flexible substrate Kapton, and the Au layer was deposited on the back of the Kapton film as an electrode. The flexible iTEAS was implanted into the pericardium of live pigs. In response to the heartbeat, the Voc and Isc of iTEAS were approximately 10 V and 0.4 μA, respectively. The output signal of iTEAS was synchronized with the ECG R-wave signal, and the output signals of the two were consistent under various pathological conditions, indicating that the iTEAS is reliable and accurate for signal monitoring during a heart attack. iTEAS also detected blood pressure and respiration. After epinephrine infusion, the peak output voltage of the iTEAS increased with increasing in blood pressure.

Ouyang et al. proposed a super-sensitive and flexible self-powered pulse sensor (SUPS) based on triboelectricity [170]. The SUPS possessed good output performance and a voltage output of 1.2 V. The SUPS was integrated with a Bluetooth chip to achieve real-time monitoring of cardiovascular pulse signals for prevention of cardiovascular diseases. In 2019, they further demonstrated a symbiotic cardiac pacemaker (SPM) based on iTENG [171], which transformed and stored energy in the body and enabled cardiac pacing in large animals. The SPM consisted of an energy-harvesting unit (iTENG), power management unit (PMU), and pacemaker unit. The iTENG was implanted between the heart and pericardium of an adult Yorkshire pig to collect biomechanical energy, and the *in vivo* Voc, Qsc, and Isc values were 65.2 V, 3.6 nC, and 0.5 μA, respectively; also, the iTENG recorded ECG signals effectively (Fig. 8**c**). The iTENG converted the mechanical energy generated by heart movement into electrical energy, which was stored in a 100 μF capacitor via a rectifier. When the external PMU was switched off, the PMU capacitor stored the converted electrical energy. The PMU can be switched on by an external magnet. Under the action of electrical energy, the cardiac pacemaker generated electrical pulses to achieve cardiac pacing and regulated the heartbeat frequency. The output voltage and duration of the electrical pulse were 3 V and 0.5 ms, which corrected sinus arrhythmia.

Liu et al. designed a self-powered intracardiac pressure sensor (SEPS) based on TENG to collect the mechanical energy of blood flow [172]. The SEPS was composed of an encapsulation layer, an electrode layer, a friction layer, and a spacer layer. The dimensions of the SEPS were about $1 \times 1.5 \times 0.1$ cm^3. The SEPS and a surgical catheter were minimally invasively implanted into the left atrium and left ventricle of a pig. *In vivo*, the SEPS responded well to LVP and LAP. Implantation of the SEPS into the left ventricle of a pig yielded stable electrocardiogram (ECG), femoral artery pressure (FAP), and SEPS signals (Fig. 8**d**). The SEPS was highly sensitive, mechanically stable, showed good linearity ($R^2 = 0.997$), and had a sensitivity of 1.195 mV mmHg^{-1}. The SEPS was miniaturized and flexible and could convert blood-flow energy in the heart cavity into an electrical signal for evaluating cardiac function.

4.2.2. Implantation of a nanogenerator into the thoracic and abdominal cavities

As mentioned above, Li et al. developed the first ZnO-based SWG to harvest energy from rat respiration in 2010 [163]. Compared with implanted on the surface of the heart, the output performance of SWG implanted on the ventral side was slightly lower, with Voc of 1 mV and Isc of 1 pA. In 2014, Zheng et al. collected energy from respiration *in vivo* using iTENG to drive a prototype pacemaker [173] (Fig. 9**a**). The dimensions of the iTENG were 1.2×1.2 cm and the contact layer area was 0.64 cm^2. *In vitro* testing showed that the Voc of the iTENG was 12 V, and the Isc was 0.25 μA. The iTENG was implanted under the skin of the left chest of a rat. As the rat inhaled and exhaled, the iTENG friction layer contacted and separated, converting the mechanical energy of respiration into an electrical signal with a voltage of 3.73 V and a current of 0.14 μA. The trend of the forced vital capacity (FVC) curve of iTENG was synchronized with the short-circuit current curve. The electrical energy generated by iTENG drove a cardiac pacemaker and stimulated the rat heart.

Li et al. developed a retractable, miniature, battery-less implantable nanogenerator (i-NG) [174]. The i-TENG had a multi-layer structure: Cu/Cr IDE was deposited on a 50 μm PET substrate as two electrode layers, and a soft silicon elastomer with a cavity design was used as the encapsulation layer. i-TENG was implanted into the abdominal cavity of rats to convert biomechanical energy into electrical energy via abdominal-muscle relaxation and contraction (Fig. 9**b**). *In vivo*, the maximum Vpp generated by one electrode pair unit was 0.4 V, whereas the output of two electrode pairs was 0.8 V. As the rat respiration frequency increased, the average output voltage of iTENG increased. The rectifier and capacitor were connected to an LED, which lit up when the potential reached ~2.2 V.

4.3. Chemotherapy based on self-driving systems

There are two types of chemotherapy based on nanogenerators: drug delivery systems and small-molecule therapies based on electrical signal conversion.

4.3.1. Self-powered drug delivery system

Body fluids are the substances with the highest content in the human body, and as a carrier, they participate in the transportation of gases, inorganic salts, and organic molecules throughout the body. When the nanogenerator interacts with body fluids, an electrolyzed water reaction will occur, and the generated gas can boost the delivery of drugs. Song et al. proposed an implantable self-powered drug delivery system (iDDS) (Fig. 10**a**). The iDDS consisted of an energy-harvesting device (TENG) and a drug-pumping system [175]. The TENG was composed of a rotor, stator, electrification material, and encapsulation material. The drug-pumping system comprised a PDMS drug reservoir, a PDMS microtube, and two Au electrodes. The pumping system, whose dimensions were $10 \times 10 \times 2$ mm^3, was suitable for subcutaneous implantation. The electrical energy generated by TENG was transmitted to the Au electrode through the wire, and the water in the pump was decomposed to O_2, and H_2 under the electrical potential, pressurizing the drug reservoir and pumping out the drug through the microtube. Fifty microliters of fluorescent particles were successfully sent to the anterior chamber of isolated pig eyes.

Red blood cells (RBCs) are natural carriers of drugs with excellent biocompatibility and bioactivities. Electrical stimulation can cause cell membrane perforation to achieve drug release. Zhao et al. developed an implantable magnet meter friction nanogenerator (MTENG) for *in vivo* tumor treatment [176]. PTFE and Ti were used as friction layers, and their backs were attracted by magnets to control their contact and separation. The Voc value of MTENG was 70 V, and the Isc was 0.55 μA. RBCs were loaded with doxorubicin (DOX) and controlled by an electric field (EF) generated by MTENG for targeted release. Following MTENG-mediated EF stimulation for 8 h, DOX release increased to 59.7%. The viability of HeLa cells treated with free DOX was 70.4%, compared to 62.7% in the free DOX+EF group. HeLa cell viability was lowest (20.9%) in the D@RBC+EF group. The antitumor effect of MTENG-controlled D@RBC DDS was investigated in BALB/c-nu mice with HeLa tumors. Long-term experiments further showed that the D@RBC EF group had the smallest tumor volume and the highest survival rate. No change in bodyweight was noted, indicating few side effects (Fig. 10**b**). DDS systems controlled by MTENG are effective for the treatment of cancer.

Since the surface charge distribution is related to the radius of curvature of the conductor, the charge tends to accumulate at the tip of the needle, forming an enhanced electric field. Therefore, by integrating the nanogenerator with nanoneedle array, the electroporation drug delivery can be significantly enhanced. Liu et al. developed a drug delivery system with a focus on perforation (Fig. 10**c**), which was driven by TENG and achieved intracellular drug delivery using nanoneedle electrodes [177]. The electric breakdown device of the in vitro drug delivery system comprised a handheld TENG, a rectifier bridge, an anode, and a cathode. The silicon nanoneedle array electrode was the anode, and the

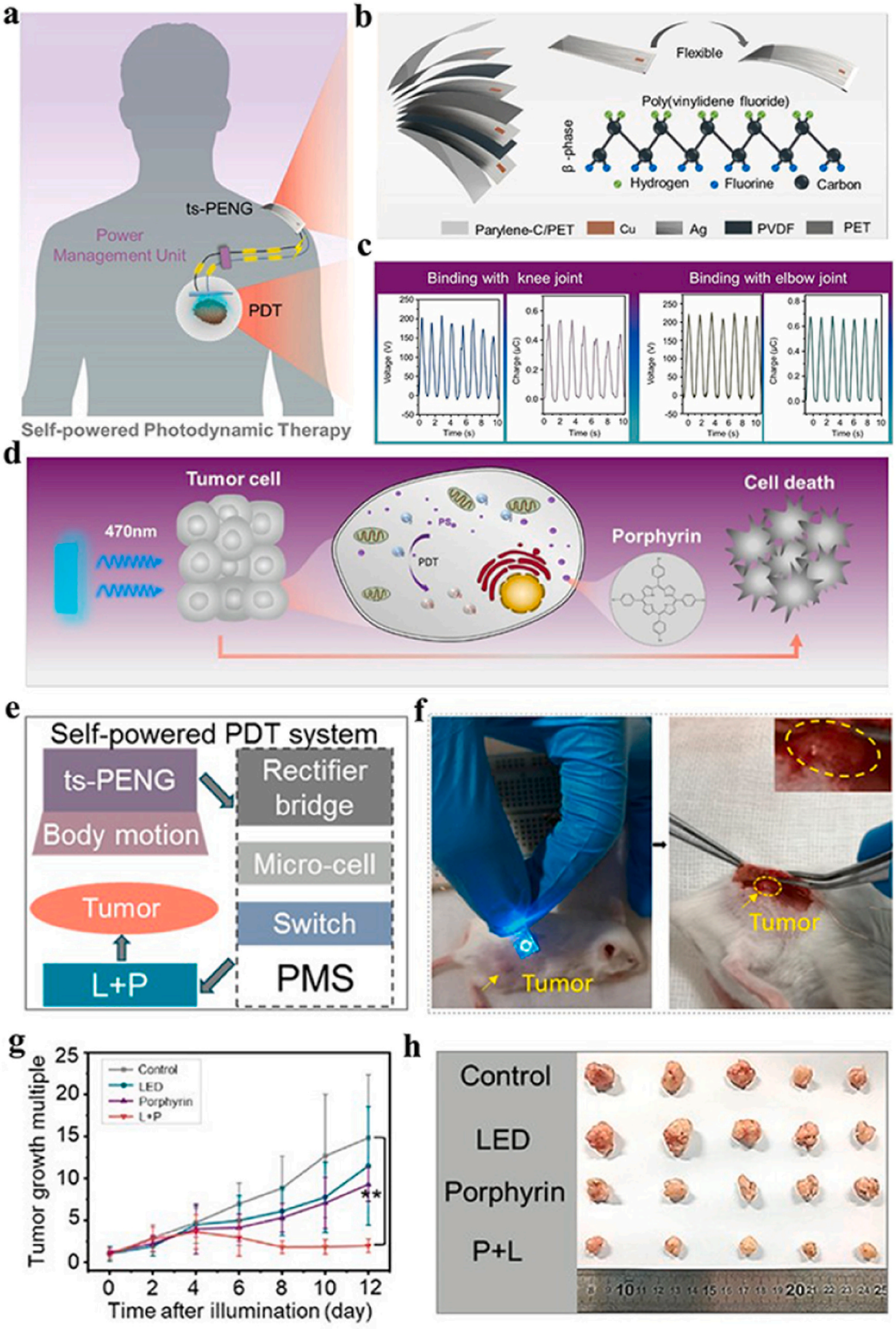

Fig. 11. An s-PDT system for long-term autonomous cancer therapy. (a) Structure and composition: ts-PENG, PMU, m-LED, and photosensitizer. (b) ts-PENG is composed of an encapsulation layer, PVDF, and a substrate layer. (c) ts-PENG fixed on the Voc and Qsc from the knee and elbow joints. (d) *In vitro*, the working mechanism of an s-PDT system. The LED is driven by ts-PENG to emit light at a wavelength of 470 nm, which kills tumor cells in combination with porphyrin. (e) Composition of each part of a self-powered s-PDT system. (f) Establishment of a tumor model and implantation of an s-PDT system in nude mice. (g) Change in tumor

growth multiple and (h) tumor volume.
(a–h) Reproduced with permission [184]. Copyright 2020, American Chemical Society.

metal Al was the electrode cathode. The measured Voc of TENG was 20 V, and the Isc was 4 μA. The electrical field simulation showed that the maximum electrical field at each nanoneedle tip could reach 2800 V cm^{-1}. TENG driven by finger friction controlled the nanoneedle to release dextran-FITC subcutaneously into mouse back. Following drug delivery in vivo, the nanoneedle was structurally intact, demonstrating the effectiveness of TENG electroporation-mediated drug delivery. Bok et al. proposed a drug delivery system based on the combination of soluble microneedles and TENG [178]. The friction layers of TENG were composed of salmon deoxyribonucleic acid (SDNA) film and polymer film. The microneedle could be dissolved in the stratum corneum, and TENG generated an electric field on the microneedle and the skin to accelerate the transdermal delivery of the drug (Fig. 10**d**). TENG generated a voltage of approximately 95 V when implanted into the skin tissue of pork. In a single microneedle system, only 50 ng of drug could be released. When the microneedle was applied with TNG, the release amount of RhB increased to ~220 ng within 60 s under 2 Hz and 0.2 MPa friction charging conditions.

Some drugs can be stably loaded on the surface of the carriers through oxidation reaction. The nanogenerators can inject the generated electrons into the carriers and undergo reduction reactions to control the release of the drugs. Ouyang et al. proposed a self-powered on-demand transdermal drug delivery system based on TENG [179]. The system included radial arrayed TENG, transdermal patch, power management circuit. Dexamethasone sodium phosphate (DEX-P) and 6-carboxyfluorescein (FLU) were loaded on the PPy porous membrane by using a one-step electro-polymerization, in which the anionic drugs interacted with the polymer matrix to balance the positive charge of PPy backbone during the polymerization of pyrrole. The drugs were released through a reduction reaction, when a negative voltage was applied to PPys. The current generated by TENG acted on the iontophoresis patch electrode, promoting the release of the drug (Fig. 10**e**). As TENG rotated manually (30–40 rpm) for 1.5 min, the drug release rate was 3 μg/cm^2. In addition, changing the charging time of TENG or the resistance of the power management circuit could accurately control the drug release rate within the range of 0.05–0.25 g/cm^2. It had been proved on pig skin that the drug delivery performance of the improved system was superior to that of traditional transdermal patches. Recently, Yang et al. further combined PPy-drug loading system with microneedle patch, and designed a self-powered controllable transdermal drug delivery system (sc-TDDS) based on PENG to achieve on-demand drug delivery [180]. The PPy film doped with Dex was deposited on the surface of microneedle, which could directly penetrate through the skin and release drug into the epidermis or dermis of skin. Under electrical stimulation produced by PENG, the sc-TDDS released 8.5 ng of dexamethasone (Dex) each time, better than the skin surface lotion. It provides new ideas for the customized treatment of psoriasis and other skin diseases.

4.3.2. Free radical therapy based on electric signal conversion

Photodynamic therapy (PDT) is a photochemical method to kill local primary and recurring tumor cells. The excited photosensitive materials transfer energy to the surrounding oxygen to generate highly active singlet oxygen, which oxidize nearby biological macromolecules and kill tumor cells [181].

The transition of photosensitive materials from the ground state to the excited state relies on the absorption of external energy. Generally, light irradiation is the mainstream way to drive PDT therapy. However, due to the limitation of the depth of tissue penetration, the implantable LED light source has received more and more attention in PDT treatment [182,183]. Nanogenerators can be coupled with implantable LEDs to realize the conversion of mechanical energy to electricity, and finally to light. Liu et al. proposed a novel self-powered photodynamic system (s-PDT) for the treatment of long-term cancer (Fig. 11**a**) [184]. The s-PDT system was composed of an energy harvester unit (ts-PENG), power management unit (PMU), m-LED, and photosensitizer (PS). The ts-PENG comprised an encapsulation layer, PET substrate, PVDF bimorphic layer, and Ag electrode. The wire was fixed to the two electrodes by Cu tape. The dimensions were about 2 cm × 6 cm × 0.5 mm, and the weight was 1.68 g (Fig. 11**b,** 11**e**). PENG attached to the knee could produce an Voc of 200 V and transfer a charge of 0.5 μC. The Voc and the amount of charge transferred by PENG at the elbow joint were 220 V and 0.65 μC, respectively (Fig. 11**c**). The cancer therapeutic mechanism of PDT is shown in Fig. 11**d**. Porphyrin acted as a photosensitizer (PS) to deliver the energy produced by the LED, thereby realizing pulsed-light stimulation (PLS) and intermittent continuous light stimulation (ICLS) therapies for cancer. PLS treatment in vitro significantly inhibited tumor cell growth by 60%. *In vivo*, ICLS had a strong killing effect on the initial tumor tissue by intermittently providing irradiation. LED+porphyrin inhibited tumor cells by 87.46% (Fig. 11**g,** 11**h**). Moreover, patients can choose the appropriate treatment plan according to disease stage. This work suggests the feasibility of a long-term photodynamic therapy device with good compliance and self-management, which overcomes the disadvantages of battery-powered PDT and the space and practical inconvenience of driving LEDs for wireless charging. Kim et al. proposed an implantable ultrasonically powered light source to trigger photodynamic therapy [185]. In addition to light radiation, photosensitive materials can also be excited by direct electron transfer. Piezoelectric material is an ideal medium for electron generation and transmission. Ultrasound with a strong tissue penetration depth is used as an external mechanical wave, which can trigger the piezoelectric effect and promote the migration of carriers to the photosensitive materials, giving rise to the generation of reactive oxygen species. Wu et al. synthesized barium titanate nanocubes with Schottky junctions modified by gold nanoparticles (Au@BTO). Au@BTO, as a new kind of sonosensitizer for sonodynamic therapy, produced reactive oxygen species under the action of ultrasound, and possessed high antibacterial efficiency against Gram-negative and Gram-positive bacteria [186].

4.4. Tissue engineering

Electrical stimulation can promote cell migration and differentiation by affecting signaling pathways, which plays a key role in tissue engineering [187] and wound healing [188]. Nanogenerators can replace traditional electrical stimulation devices and will realize portable, self-powered, wearable, and implantable tissue-repair systems based on electrical stimulation.

Tang et al. developed an implantable self-powered laser therapy system (SPLC) [189], which promoted the proliferation and differentiation of mouse embryonic osteoblasts (Fig. 12**a**). The SPLC consisted of a flexible TENG and an in vitro laser excitation unit. The friction layers of arch-shaped flexible TENG were composed of a PDMS film and ITO. TENG was implanted between the mouse diaphragm and liver, and the movement of the diaphragm drove TENG to generate electrical energy with a short-circuit current of 0.06 nA and open-circuit voltage of 0.2 V. The ALP level in the TENG laser treatment group increased by 16.9%, indicating bone matrix synthesis and MC3T3-E1 extracellular matrix maturation. Irradiation by the TENG laser increased mineral deposits in MC3T3-E1 cells, indicating that TENG laser treatment promoted osteoblast proliferation, differentiation, and bone formation.

Li et al. designed a photothermally adjustable biodegradable implantable friction nanogenerator (BD-iTENG) by employing Au nanorods (AuNRs) [190]. To increase the contact area between the friction layers of BD-iTENG, a hemispheres-array-structured layer was

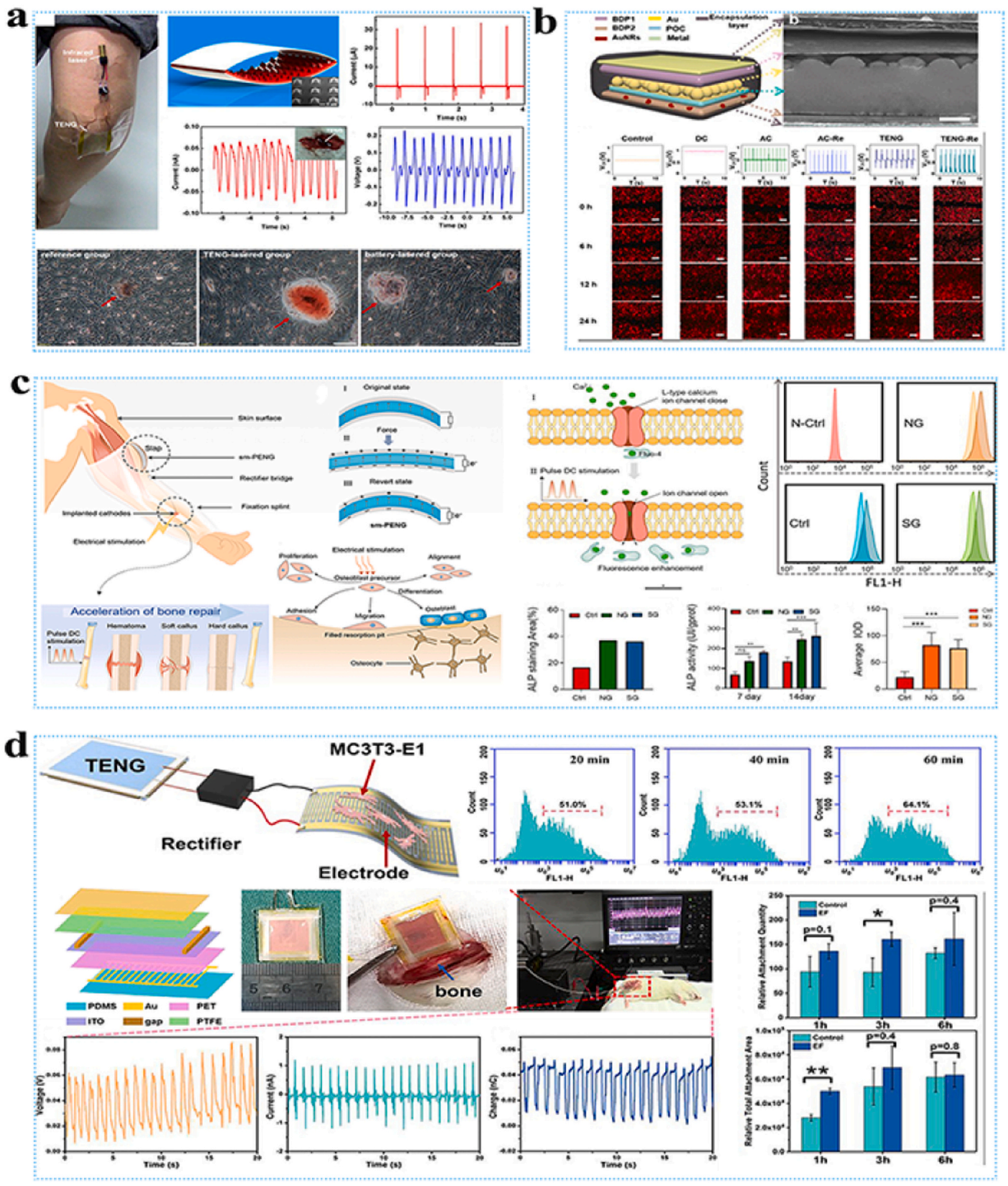

Fig. 12. Applications of nanogenerators in tissue engineering. (a) A self-powered low-intensity laser osteogenesis system based on a triboelectric nanogenerator. (b) A triboelectric nanogenerator capable of photothermal tunable degradation for tissue repair. (c) An sm-PENG system promotes bone formation by MC3T3-E1 cells. (d) A self-powered flexible implantable electrical stimulator used to induce osteoblast differentiation and bone remodeling. It consists of a triboelectric nanogenerator (TENG) and flexible interdigital electrodes.

(a) Reproduced with permission [189]. Copyright 2015, American Chemical Society. (b) Reproduced with permission [190]. Copyright 2018, Elsevier. (c) Reproduced with permission [192]. Copyright 2021, Elsevier. (d) Reproduced with permission [193]. Copyright 2019, Elsevier.

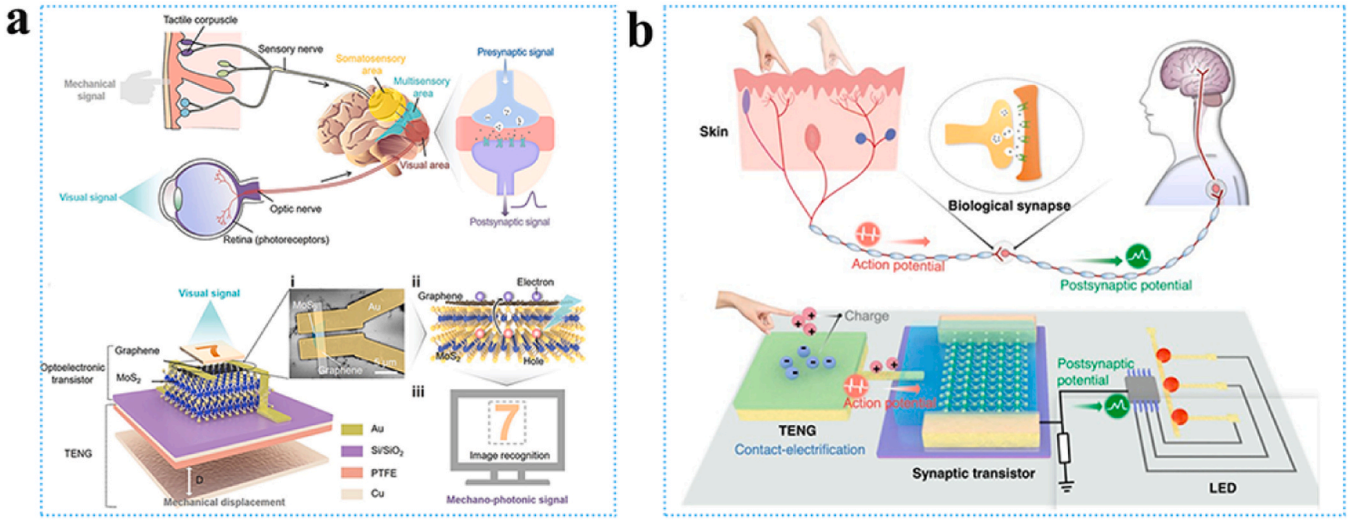

Fig. 13. (a) A mechanical-photonic artificial synapse based on a graphene/MoS_2 (Gr/MoS_2) heterojunction. (b) Contact-electrification-activated artificial afferents at femtojoule energy based on TENG.
(a) Reproduced according to the terms of the CC-BY license [195]. (b) Reproduced according to the terms of the CC-BY license [196].

used. The degradable polymer layer doped with AuNRs served as the bottom substrate. The BD-iTENG had strong mechanical energy conversion ability with a Voc of 28 V and Isc of 220 nA in vitro, and the Voc was about 2 V in vivo. The implanted AuNRs-BD-iTENG functioned for more than 28 days without near-infrared (NIR) treatment. Following NIR application, Au NRs in BD-iTENG accelerated degradation of the device through photothermal effect. The output signal of AuNRs-BD-iTENG dropped to 0 rapidly, and the device was largely degraded within 14 days. The BD-iTENG possessed great potential in tissue repairing. The output signal of BD-iTENG promoted fibroblast cells migration across the scratches, which was conductive to wound healing (Fig. 12**b**). Recently, Yao et al. developed a self-powered implantable and bioresorbable electrostimulation bone fracture healing device, which consisted of a TENG and a pair of dressing electrodes [191]. The device enabled attach to irregular tissue surface and generated stable biphasic electrical pulses through the movement of the knee joint. Under the treatment of the electrostimulation device, the fracture can be recovered within 6 weeks, and the mineral density and flexural strength were increased by 27% and 83% respectively, compared with the nonintervention group. The entire device underwent rapid autocatalytic hydrolysis and degradation in vitro, and disappeared within 18 weeks. The degradation rate *in vivo* was even faster (14 weeks), which might due to the dynamic environment in the animal body.

Zhang et al. proposed a memory piezoelectric nanogenerator (sm-PENG) to enhance bone formation and healing (Fig. 12**c**) [192]. An sm-PENG and fracture splint comprised a self-powered electrical stimulation system. Electrical stimulation promoted cell proliferation and differentiation. Tian et al. designed an electrical stimulation system based on a self-powered triboelectric nanogenerator to stimulate osteoblast differentiation [193] (Fig. 12**d**). The device consisted of a triboelectric nanogenerator, a rectifier, and interdigital electrodes. The triboelectric nanogenerator used Al and PTFE as the friction layer, Au as one of the electrode layers, and Al as the other electrode layer. Rectified pulsed direct current stimulation significantly improved the adhesion and proliferation of MC3T3-E1 cells. Markers of osteogenic differentiation, such as intracellular Ca^{2+} concentration and alkaline phosphatase expression, also improved. TENG implanted on the surface of rat femur converted the mechanical energy generated by exercise into electrical energy, which can be used for in situ treatment. The above suggest the broad application prospects of nanogenerators in tissue engineering, such as bone regeneration and bone healing.

4.5. *Artificial tactile/visual neural networks*

Nanogenerators can simulate artificial retina systems and enable image recognition and signal perception and transmission [194]. Yu et al. designed a highly plastic artificial synapse based on advanced animal touch/visual neural network conduction and the high electron mobility and strong photoelectric response of graphene/MoS_2 (Cr/MoS_2) (Fig. 13**a**) [195]. The synapse system was composed of a phototransistor based on a graphene/MoS_2 (Cr/MoS_2) heterostructure and a triboelectric nanogenerator in contact separation mode. The Cr/MoS_2 heterostructure phototransistor was divided into three parts: Si/SiO_2 substrate, multilayer MoS_2 grown on the substrate, and single-layer graphene covering MoS_2. In the triboelectric nanogenerator, one side of the Cu electrode and PTFE served as the friction layer, and the triboelectric potential drove the photoelectric behavior of synapses. The triboelectric potential was equivalent to presynaptic stimulation, and the electrical signal output between the source and drain simulated the post-synaptic current (PSC). The heterostructure of MoS_2 controlled charge exchange, similar to neurotransmitter release in human synapses. An increase in light intensity enhanced the PSC of the mechanical photonic artificial synapse, and the PSC remained relatively stable as the light intensity decreased. Inspired by the three-layer neural network of the retina, a three-layer artificial neural network was designed, and showed an image recognition accuracy rate of 92%. The mechanical-photonic artificial synapse has multiple modes of interaction, promoting advanced neural network simulation and interactive artificial intelligence with high plasticity.

Inspired by the transmission of biological neuroelectric signals between synapses, Yu et al. simulated and designed artificial afferents based on triboelectric nanogenerators (Fig. 13**b**) [196]. The afferent nerve was composed of self-activating components, protruding transistors, and functional circuits. The triboelectric potential generated by the TENG was used to activate the protruding transistor and transmit the mechanical signal to the functional area. The device consisted of an incoming neuron, a microcontroller unit (MCU), and two sets of LEDs connected in series. Operation of the LEDs confirmed the dynamic logic function of artificial afferents. When different triboelectric potentials activated synaptic transistors, different post-synaptic currents (EPSC) were generated, producing different bias voltage signals by shunt circuits. As the touch potential generated by Teng-1 (2×2 cm^2) increased to > 2 V, the EPSC was > 30 nA. The converted bias voltage signal was > 0.5 V, and the red LED lit up. When the touch voltage generated by

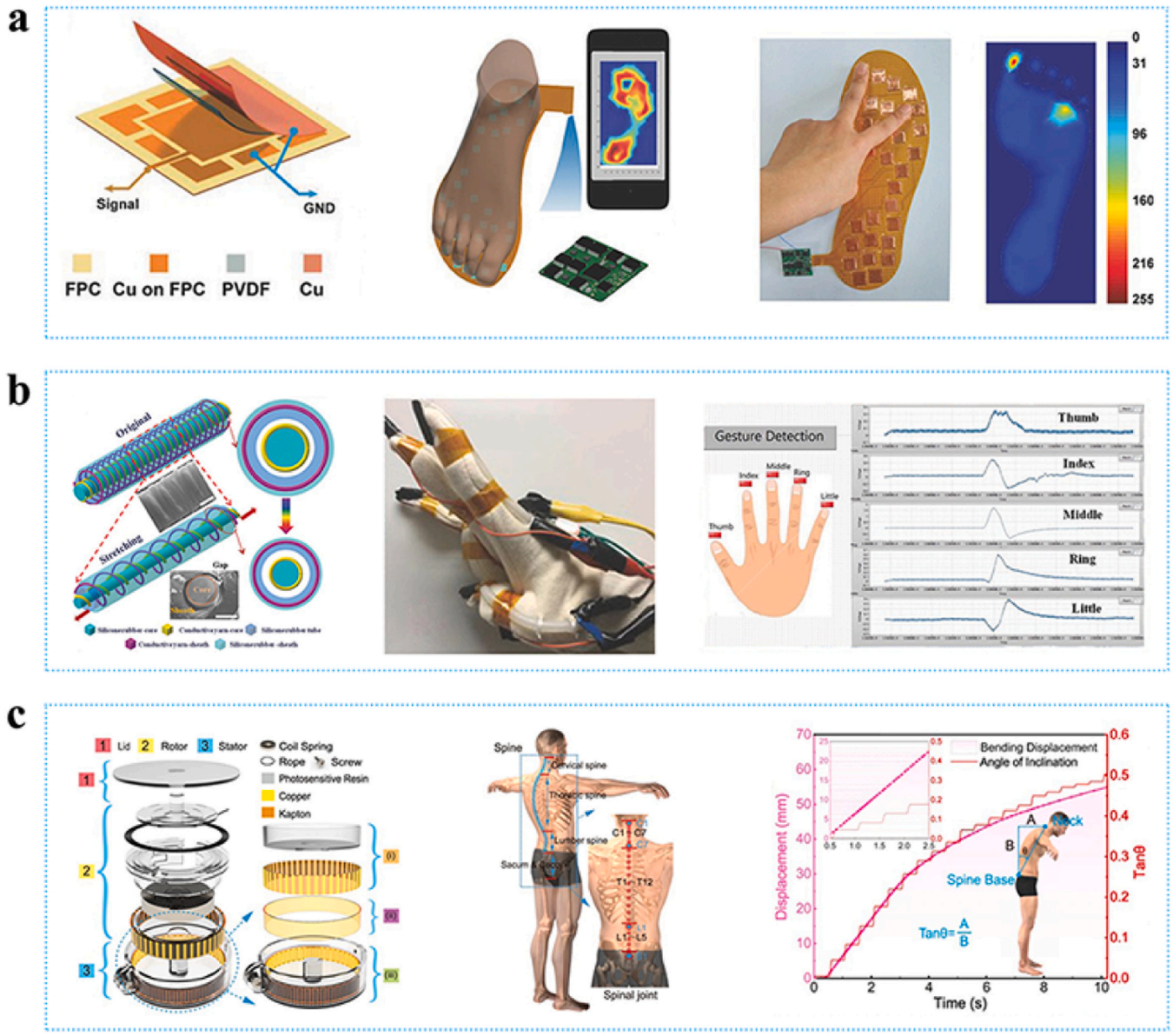

Fig. 14. (a) A plantar pressure monitoring system with two-point contact. (b) Smart gloves containing yarn-based TENG, and the voltage output signal was realized by the swing of five fingers. (c) A stretch sensor and its measurement of the inclination angle from the bottom of the spine to the neck.
(a) Reproduced with permission [197]. Copyright 2018, John Wiley & Sons. (b) Reproduced with permission [198]. Copyright 2018, John Wiley & Sons. (c) Reproduced according to the terms of the CC-BY license [199].

Teng-2 ($1.5 \times 1.5\ cm^2$) was < 2 V, the corresponding EPSC was < 30 nA, and the generated bias voltage was < 0.5 V, triggering operation of a green LED. Therefore, in touch mode, automatically activated artificial afferents can identify spatiotemporal signals.

4.6. Motion correction and training

Human motions with various amplitudes and velocities ranging from slight movement to full-body kinematics, are full of diverse and important physiological health information which are closely related to various kinds of diseases. There are several works based on wearable nanogenerators have been done to monitor movement status and identify movement disorders.

Deng et al. fabricated a self-powered smart insole plantar pressure mapping system based on hybrid nanogenerators (Fig. 14**a**) [197]. The device was sensitive to the variation of pressure and shows great measurement span up to 200 kPa. Integrated with the Bluetooth technology, the foot pressure signal measured by NGs could be shown in the phone in time. The device has great potential in footwear design, information acquisition, sport/exercise biomechanics, diabetes ulceration prediction, as well as injury prevention. In 2018, based on core–sheath structure, a multifunctional yarn-based TENG was designed (Fig. 14**b**) [198]. The device was stretchable, washable, flexible, stable and reliable. It had been applied in movement measurement, gesture recognizing, and so on. It would be essential to real-time self-powered human-interactive sensing in future. Furthermore, Wang's group provided a grating-structured TENG and applied it in the monitoring of human's joint motions and the real-time spinal bending/stretching in a sagittal plane (Fig. 14**c**) [199]. The equipment is beneficial to reduce the risks of spinal disorders and could be fabricated into rehabilitation brace for real-time recording of patients' joint motions after surgery.

Table 1
Summary of the biomedical application of NGs.

	Modulation of neural activity [157–162]	Cardiovascular system [163–174]	Chemotherapy [175–186]	Tissue engineering [187–193]	Artificial tactile/visual neural network [194–196]	Motion correction and training [197–199]
Device Size	4.0 cm × 4.0 cm × 20.0 μm [157] 3.0 cm × 1.8 cm × 0.25 mm [158] 1.7 cm × 1.7 cm 4.0 cm × 4.0 cm (Max) [159] 16.0 × 12.0 × 2.5 mm^3 [161] 4.0 cm × 4.0 cm [162]	1.0 cm × 1.0 cm [166] 25 mm × 10 mm × 1.5 mm [168] 30.0 × 20.0 × 1.0 mm^3 [169] 1.0 cm × 1.5 cm × 0.1 cm [172] 1.2 cm × 1.2 cm/3.0 cm × 2.0 cm [173] 1.1 cm × 3.5 cm × 0.8 mm [174]	10 mm × 10 mm × 2 mm [175] diameter of the friction layers: 2.5 cm [176] freestanding 4 × 5.5 cm contact-separation 4 × 4 cm [177] 1.5 cm × 2.0 cm and 2.0 cm × 3.0 cm [178] 0.5 cm × 0.5 cm [179] 7.5 cm × 3.5 cm [180] 2.0 cm × 6.0 cm × 0.5 mm [182]	diameter 2 cm, thickness 2 mm [188] 1.5 cm × 1.0 cm [189] 1.2 cm × 1.2 cm thickness 0.65 mm [190] 35 × 15 × 0.45 mm^3 [191] 55 × 25 × 0.3 mm^3 [192] 2.0 cm × 2.0 cm [193]	length 60 mm thickness 10 μm [194] TENG-1 2 × 2 cm^2 TENG-2 1.5 × 1.5 cm^2 [196]	13.5 mm × 13.5 mm × 0.3 mm [197] 4 cm × 6.5 cm [199]
Sensitivity/ Output voltage	0.26 V [158] 11 V [159] 160 V [160] 0.05–0.12 V [161]	3 mV [163] 4.5 V [164] 3 V [165] 17.8 V [166] 14 V [168] 10 V [169] 1.2 V [170] 65.2 V [171] 78.6 mV [172] 3.73 V [173] 2.2 V [174]	15 V [175] 70 V [176] 20 V [177] 95 V [178] 100 V [179,180] 200 V [184]	0.25–1.8 V [188] 115 V [189] 28 V [190] ~4 V [191] 78 V [192] 100 V [193]	1.45 V (peak) [194] 62 to − 52 V [195] TENG-1 0.75 V TENG-2 0.3 V [196]	1.6 V [197] 19 V (different compressing frequencies)/ 13.5 V (fixed tensile strain of 100%) [198] ~20–30 V [199]
Position	mouse brain [157–159] sciatic nerve [160] stomach wall of rats [161]	heart [163,164,166] lung [164] diaphragm [164] anterior wall of the apex [165] between the heart and the pericardium [168,171] Pericardium [169] left ventricle [172] under the thoracic skin [173] abdominal cavity [174]	ex vivo ocular [175] HeLa cells [176] MCF-7 cells [177] Porcine cadaver skin [178] porcine skin [179] skin of SD rats [180] tumor cells [184]	skin of Female BALB/c mice [188] MC3T3-E1 [189,192] L929 cells [190] between the knee joint and the hip of SD rat [191] bone surface [193]	mimic sensory nerve system [194] artificial synapse [195] artificial afferent [196]	insole [197] smart glove [198] spine/knee/arm/neck/waist [199]
Types of NGs	PENG [159] TENG [157,158,160–162]	PENG [163–166] TENG [168,169,171–174]	PENG [180,184] TENG [175–179]	PENG [187,188,192] TENG [189–191,193]	PENG [194] TENG [195,196]	PENG [197] TENG [198,199]
Materials	PDMS/PPy [157,158] PIMNT [159] PDMS/Cu [160] PTFE/Cu [161] PTFE/Al [162]	ZnO [163] PZT [162,165] PMN-PZT [166] PTFE/Al [168,169,171,172] PDMS/Al [173] PTFE/ Cu/Cr IDEs [174]	PTFE/Cu [175,177,179] PTFE/Ti [176] SDNA/polyimide [178] PVDF [180,184]	P(VDF-TrFE) [187] PDMS/ITO [189] BDP1/ POC [190] PVDF [188,192] PTFE/Al [193]	P(VDF-TrFE) [194] PTFE/Cu [195] PTFE/Al [196]	PVDF [197] conductive yarn/silicone rubber [198] Copper/Kapton [199]

5. Conclusion and outlook

Nanogenerators make full use of potential biomechanical energy, which facilitates progress in biomedicine. This article reviews the basic principles, materials, and design of nanogenerators, as well as their applications in neurology, cardiology, drug delivery, and tissue engineering, etc (Table 1). Nanogenerators are useful for clinical research because of their self-driving, portability, and Internet-of-Things connection potential. However, several issues need to be resolved in future. Firstly, the development of implantable nanogenerators is inseparable from discovery of high-performance, lightweight materials with good biocompatibility, flexibility, mechanical stability, and stable electrical output. Improved materials and device performance will expand the applications of nanogenerators. Corrosion and wear of nanogenerators (especially TENG) under physiological conditions are important. It is essential to explore packaging layer materials with greater environmental tolerance and universality and develop new device packaging technology to improve device stability and service life. Secondly, for implantable devices, material degradation, metabolism, and potential immunogenicity need to be studied. This will promote the development of transient electronic devices and accelerate research on controllable degradation of degradable electronics. Finally, the electrical signals generated by cells and tissues are widely present in living bodies, but humans have little knowledge about the relationship between electricity and life. Therefore, it can be expected that nanogenerators can broaden our understanding of life and achieve a wider range of applications in the field of life detection and regulation.

Declaration of Competing Interest

The authors declare that they have no known competing financial interests or personal relationships that could have appeared to influence the work reported in this paper.

Acknowledgements

Mingjun Sun and Zhe Li contributed equally to this paper. The authors are grateful for the support received from the National Natural Science Foundation of China (No. T2125003, 51902344, 61875015, 81871492), Beijing Natural Science Foundation (JQ20038), Projects of Ten-Thousand Talents Program No. QNBJ2019-2, Key R & D Plan of Ningxia Hui Autonomous Region No. 2020BCG01001.

References

[1] Y. Long, J. Li, F. Yang, J.Y. Wang, X.D. Wang, Wearable and implantable electroceuticals for therapeutic electrostimulations, Adv. Sci. 8 (2021), 2004023.
[2] Y.C. Lai, Y.C. Hsiao, H.M. Wu, Z.L. Wang, Waterproof fabric-based multifunctional triboelectric nanogenerator for universally harvesting energy from raindrops, wind, and human motions and as self-powered sensors, Adv. Sci. 6 (2019), 1801883.
[3] H.M. Yang, F.R. Fan, Y. Xi, W.Z. Wu, Bio-derived natural materials based triboelectric devices for self-powered ubiquitous wearable and implantable intelligent devices, Adv. Sustain. Syst. 4 (2020), 2000108.
[4] S. Azimi, A. Golabchi, A. Nekookar, S. Rabbani, M.H. Amiri, K. Asadi, M. M. Abolhasani, Self-powered cardiac pacemaker by piezoelectric polymer nanogenerator implant, Nano Energy 83 (2021), 105781.
[5] S. Lee, H. Wang, J.H. Wang, Q.F. Shi, S.C. Yen, N.V. Thakor, C. Lee, Battery-free neuromodulator for peripheral nerve direct stimulation, Nano Energy 50 (2018) 148–158.
[6] S. Lee, H. Wang, W.Y. Xian Peh, T. He, S.-C. Yen, N.V. Thakor, C. Lee, Mechano-neuromodulation of autonomic pelvic nerve for underactive bladder: a triboelectric neurostimulator integrated with flexible neural clip interface, Nano Energy 60 (2019) 449–456.
[7] F. Arab Hassani, R.P. Mogan, G.G.L. Gammad, H. Wang, S.-C. Yen, N.V. Thakor, C. Lee, Toward self-control systems for neurogenic underactive bladder: a triboelectric nanogenerator sensor integrated with a bistable micro-actuator, ACS Nano 12 (2018) 3487–3501.
[8] A. Sultana, M.M. Alam, S. Garain, T.K. Sinha, T.R. Middya, D. Mandal, An effective electrical throughput from PANI supplement ZnS nanorods and PDMS-based flexible piezoelectric nanogenerator for power up portable electronic devices: an alternative of MWCNT filler, ACS Appl. Mater. Interfaces 7 (2015) 19091–19097.
[9] X.J. Pu, H.Y. Guo, J. Chen, X. Wang, Y. Xi, C.G. Hu, Z.L. Wang, Eye motion triggered self-powered mechnosensational communication system using triboelectric nanogenerator, Sci. Adv. 3 (2017), 1700694.
[10] F. Ali, W. Raza, X.L. Li, H. Gul, K.H. Kim, Piezoelectric energy harvesters for biomedical applications, Nano Energy 57 (2019) 879–902.
[11] Z. Liu, H. Li, B.J. Shi, Y.B. Fan, Z.L. Wang, Z. Li, Wearable and implantable triboelectric nanogenerators, Adv. Funct. Mater. 29 (2019), 1808820.
[12] Z. Li, Q. Zheng, Z.L. Wang, Z. Li, Nanogenerator-based self-powered sensors for wearable and implantable electronics, Research 2020 (2020), 8710686.
[13] D.J. Jiang, B.J. Shi, H. Ouyang, Y.B. Fan, Z.L. Wang, Z. Li, Emerging implantable energy harvesters and self-powered implantable medical electronics, ACS Nano 14 (2020) 6436–6448.
[14] L.M. Zhao, H. Li, J.P. Meng, Z. Li, The recent advances in self-powered medical information sensors, Infomat 2 (2020) 212–234.
[15] D.J. Jiang, B.J. Shi, H. Ouyang, Y.B. Fan, Z.L. Wang, Z.M. Chen, Z. Li, A 25-year bibliometric study of implantable energy harvesters and self-powered implantable medical electronics researches, Mater. Today Energy 16 (2020), 100386.
[16] S.Y. Huang, Y. Liu, Y. Zhao, Z.F. Ren, C.F. Guo, Flexible electronics: stretchable electrodes and their future, Adv. Funct. Mater. 29 (2019), 1805924.
[17] Y.J. Hong, H. Jeong, K.W. Cho, N. Lu, D.H. Kim, Wearable and implantable devices for cardiovascular healthcare: from monitoring to therapy based on flexible and stretchable electronics, Adv. Funct. Mater. 29 (2019), 1808247.
[18] R. Hinchet, S.W. Kim, Wearable and implantable mechanical energy harvesters for self-powered biomedical systems, ACS Nano 9 (2015) 7742–7745.
[19] M.F. Paton, M. Landolina, J.R. Billuart, D. Field, J. Sibley, K. Witte, Projected longevities of cardiac implantable defibrillators: a retrospective analysis over the period 2007-17 and the impact of technological factors in determining longevity, EP Eur. 22 (2020) 149–155.
[20] A. Ahmed, I. Hassan, T. Ibn-Mohammed, H. Mostafa, I.M. Reaney, L.S.C. Koh, J. Zu, Z.L. Wang, Environmental life cycle assessment and techno-economic analysis of triboelectric nanogenerators, Energy Environ. Sci. 10 (2017) 653–671.
[21] M.J. Guan, W.H. Liao, On the efficiencies of piezoelectric energy harvesting circuits towards storage device voltages, Smart Mater. Struct. 16 (2007) 498–505.
[22] X.D. Wang, J.H. Song, J. Liu, Z.L. Wang, Direct-current nanogenerator driven by ultrasonic waves, Science 316 (2007) 102–105.
[23] D. Jiang, B. Shi, H. Ouyang, Y. Fan, Z.L. Wang, Z. Li, Emerging implantable energy harvesters and self-powered implantable medical electronics, ACS Nano 14 (2020) 6436–6448.
[24] L. Huang, S. Lin, Z. Xu, H. Zhou, J. Duan, B. Hu, J. Zhou, Fiber-based energy conversion devices for human-body energy harvesting, Adv. Mater. 32 (2020), 1902034.
[25] R. Sahoo, S. Mishra, L. Unnikrishnan, S. Mohanty, S. Mahapatra, S.K. Nayak, S. Anwar, A. Ramadoss, Enhanced dielectric and piezoelectric properties of Fe-doped ZnO/PVDF-TrFE composite films, Mater. Sci. Semicond. Process. 117 (2020), 105173.
[26] L. Zhang, S. Bai, C. Su, Y.B. Zheng, Y. Qin, C. Xu, Z.L. Wang, A high-reliability kevlar fiber-ZnO nanowires hybrid nanogenerator and its application on self-powered UV detection, Adv. Funct. Mater. 25 (2015) 5794–5798.
[27] G. Murillo, A. Blanquer, C. Vargas-Estevez, L. Barrios, E. Ibanez, C. Nogues, J. Esteve, Electromechanical nanogenerator-cell interaction modulates cell activity, Adv. Mater. 29 (2017), 1605048.
[28] Y.Y. Zhao, P. Deng, Y.X. Nie, P.L. Wang, Y. Zhang, L.L. Xing, X.Y. Xue, Biomolecule-adsorption-dependent piezoelectric output of ZnO nanowire nanogenerator and its application as self-powered active biosensor, Biosens. Bioelectron. 57 (2014) 269–275.
[29] Z.L. Wang, ZnO nanowire and nanobelt platform for nanotechnology, Mat. Sci. Eng. R 64 (2009) 33–71.
[30] R. Hinchet, H.J. Yoon, H. Ryu, M.K. Kim, E.K. Choi, D.S. Kim, S.W. Kim, Transcutaneous ultrasound energy harvesting using capacitive triboelectric technology, Science 365 (2019) 491–494.
[31] K.I. Park, J.H. Son, G.T. Hwang, C.K. Jeong, J. Ryu, M. Koo, I. Choi, S.H. Lee, M. Byun, Z.L. Wang, K.J. Lee, Highly-efficient, flexible piezoelectric PZT thin film nanogenerator on plastic substrates, Adv. Mater. 26 (2014) 2514–2520.
[32] S. Liu, D. Zou, X. Yu, Z. Wang, Z. Yang, Transfer-free PZT thin films for flexible nanogenerators derived from a single-step modified sol-gel process on 2D mica, ACS Appl. Mater. Interfaces 12 (2020) 54991–54999.
[33] D.Y. Park, D.J. Joe, D.H. Kim, H. Park, J.H. Han, C.K. Jeong, H. Park, J.G. Park, B. Joung, K.J. Lee, Self-powered real-time arterial pulse monitoring using ultrathin epidermal piezoelectric sensors, Adv. Mater. 29 (2017), 1702308.
[34] C. Zhu, D. Guo, D. Ye, S. Jiang, Y. Huang, Flexible PZT-integrated, bilateral sensors via transfer-free laser lift-off for multimodal measurements, ACS Appl. Mater. Interfaces 12 (2020) 37354–37362.
[35] C. Dagdeviren, F. Javid, P. Joe, T. von Erlach, T. Bensel, Z. Wei, S. Saxton, C. Cleveland, L. Booth, S. McDonnell, J. Collins, A. Hayward, R. Langer, G. Traverso, Flexible piezoelectric devices for gastrointestinal motility sensing, Nat. Biomed. Eng. 1 (2017) 807–817.
[36] Z. Yang, S. Zhou, J. Zu, D. Inman, High-performance piezoelectric energy harvesters and their applications, Joule 2 (2018) 642–697.
[37] S. Selvarajan, A. Kim, S.H. Song, Biodegradable piezoelectric transducer for powering transient implants, IEEE Access 8 (2020) 68219–68225.
[38] H.X. Su, X.B. Wang, C.Y. Li, Z.F. Wang, Y.H. Wu, J.W. Zhang, Y.Z. Zhang, C. L. Zhao, J.G. Wu, H.W. Zheng, Enhanced energy harvesting ability of

polydimethylsiloxane-$BaTiO_3$-based flexible piezoelectric nanogenerator for tactile imitation application, Nano Energy 83 (2021), 105809.
[39] S. Qian, L. Qin, J. He, N. Zhang, J. Qian, J. Mu, W. Geng, X. Hou, X. Chou, A lead-free stretchable piezoelectric composite for human motion monitoring, Mater. Lett. 261 (2020), 127119.
[40] L. Jiang, Y. Yang, R. Chen, G. Lu, R. Li, J. Xing, K.K. Shung, M.S. Humayun, J. Zhu, Y. Chen, Q. Zhou, Abnormal corpus callosum induced by diabetes impairs sensorimotor connectivity in patients after acute stroke, Eur. Radiol. 29 (2019) 115–123.
[41] C.K. Jeong, J.H. Han, H. Palneedi, H. Park, G.-T. Hwang, B. Joung, S.-G. Kim, H. J. Shin, I.-S. Kang, J. Ryu, K.J. Lee, Comprehensive biocompatibility of nontoxic and high-output flexible energy harvester using lead-free piezoceramic thin film, APL Mater. 5 (2017), 074102.
[42] X. Yu, X. Liang, R. Krishnamoorthy, W. Jiang, L. Zhang, L. Ma, P. Zhu, Y. Hu, R. Sun, C.-P. Wong, Transparent and flexible hybrid nanogenerator with welded silver nanowire networks as the electrodes for mechanical energy harvesting and physiological signal monitoring, Smart Mater. Struct. 29 (2020), 045040.
[43] S. Gupta, R. Bhunia, B. Fatma, D. Maurya, D. Singh, Prateek, R. Gupta, S. Priya, R. K. Gupta, A. Garg, Multifunctional and flexible polymeric nanocomposite films with improved ferroelectric and piezoelectric properties for energy generation devices, ACS Appl. Energy Mater. 2 (2019) 6364–6374.
[44] N. Adadi, M. Yadid, I. Gal, M. Asulin, R. Feiner, R. Edri, T. Dvir, Electrospun fibrous PVDF-TrFe scaffolds for cardiac tissue engineering, differentiation, and maturation, Adv. Mater. Technol. 5 (2020), 1900820.
[45] A. Wang, Z. Liu, M. Hu, C. Wang, X. Zhang, B. Shi, Y. Fan, Y. Cui, Z. Li, K. Ren, Piezoelectric nanofibrous scaffolds as in vivo energy harvesters for modifying fibroblast alignment and proliferation in wound healing, Nano Energy 43 (2018) 63–71.
[46] T. Huang, Y.J. Zhang, P. He, G. Wang, X.X. Xia, G.Q. Ding, T.H. Tao, "Self-matched" tribo/piezoelectric nanogenerators using vapor-induced phase-separated poly(vinylidene fluoride) and recombinant spider silk, Adv. Mater. 32 (2020), 1907336.
[47] B.Y. Lee, J.X. Zhang, C. Zueger, W.J. Chung, S.Y. Yoo, E. Wang, J. Meyer, R. Ramesh, S.W. Lee, Virus-based piezoelectric energy generation, Nat. Nanotechnol. 7 (2012) 351–356.
[48] V. Nguyen, R. Zhu, K. Jenkins, R.S. Yang, Self-assembly of diphenylalanine peptide with controlled polarization for power generation, Nat. Commun. 7 (2016) 1–6.
[49] J.H. Lee, K. Heo, K. Schulz-Schonbagen, J.H. Lee, M.S. Desai, H.E. Jin, S.W. Lee, Diphenylalanine peptide nanotube energy harvesters, ACS Nano 12 (2018) 8138–8144.
[50] F.R. Fan, L. Lin, G. Zhu, W.Z. Wu, R. Zhang, Z.L. Wang, Transparent triboelectric nanogenerators and self-powered pressure sensors based on micropatterned plastic films, Nano Lett. 12 (2012) 3109–3114.
[51] H.H. Zhang, P. Zhang, W.K. Zhang, A high-output performance mortise and tenon structure triboelectric nanogenerator for human motion sensing, Nano Energy 84 (2021), 105933.
[52] H. Li, Y.J. Zhang, Y.H. Wu, H. Zhao, W.C. Wang, X. He, H.W. Zheng, A stretchable triboelectric nanogenerator made of silver-coated glass microspheres for human motion energy harvesting and self-powered sensing applications, Beilstein J. Nanotechnol. 12 (2021) 402–412.
[53] Y. Jiang, K. Dong, J. An, F. Liang, J. Yi, X. Peng, C. Ning, C.Y. Ye, Z.L. Wang, UV-protective, self-cleaning, and antibacterial nanofiber-based triboelectric nanogenerators for self-powered human motion monitoring, ACS Appl. Mater. Interfaces 13 (2021) 11205–11214.
[54] Z.H. Lin, G. Cheng, W.Z. Wu, K.C. Pradel, Z.L. Wang, Dual-mode triboelectric nanogenerator for harvesting water energy and as a self-powered ethanol nanosensor, ACS Nano 8 (2014) 6440–6448.
[55] B.K. Yun, H.S. Kim, Y.J. Ko, G. Murillo, J.H. Jung, Interdigital electrode based triboelectric nanogenerator for effective energy harvesting from water, Nano Energy 36 (2017) 233–240.
[56] J.H. Nie, T. Jiang, J.J. Shao, Z.W. Ren, Y. Bai, M. Iwamoto, X.Y. Chen, Z.L. Wang, Motion behavior of water droplets driven by triboelectric nanogenerator, Appl. Phys. Lett. 112 (2018), 183701.
[57] L. Yang, Y.F. Wang, Y.J. Guo, W.L. Zhang, Z.B. Zhao, Robust working mechanism of water droplet-driven triboelectric nanogenerator: triboelectric output versus dynamic motion of water droplet, Adv. Mater. Interfaces 6 (2019), 1901547.
[58] S.X. Nie, H.Y. Guo, Y.X. Lu, J.T. Zhuo, J.L. Mo, Z.L. Wang, Superhydrophobic cellulose paper-based triboelectric nanogenerator for water drop energy harvesting, Adv. Mater. Technol. 5 (2020), 2000454.
[59] H. Ryu, J.H. Lee, U. Khan, S.S. Kwak, R. Hinchet, S.W. Kim, Sustainable direct current powering a triboelectric nanogenerator via a novel asymmetrical design, Energy Environ. Sci. 11 (2018) 2057–2063.
[60] Y. Xi, H. Guo, Y. Zi, X. Li, J. Wang, J. Deng, S. Li, C. Hu, X. Cao, Z.L. Wang, Multifunctional TENG for blue energy scavenging and self-powered wind-speed sensor, Adv. Energy Mater. 7 (2017), 1602397.
[61] W.H. Xu, H.X. Zheng, Y. Liu, X.F. Zhou, C. Zhang, Y.X. Song, X. Deng, M. Leung, Z.B. Yang, R.X. Xu, Z.L. Wang, X.C. Zeng, Z.K. Wang, A droplet-based electricity generator with high instantaneous power density, Nature 578 (2020) 392–396.
[62] K. Tao, H. Yi, Y. Yang, H. Chang, J. Wu, L. Tang, Z. Yang, N. Wang, L. Hu, Y. Fu, J. Miao, W. Yuan, Origami-inspired electret-based triboelectric generator for biomechanical and ocean wave energy harvesting, Nano Energy 67 (2020), 104197.
[63] C.G. Zhang, L. Liu, L.L. Zhou, X. Yin, X.L. Wei, Y.X. Hu, Y.B. Liu, S.Y. Chen, J. Wang, Z.L. Wang, Self-powered sensor for quantifying ocean surface water waves based on triboelectric nanogenerator, ACS Nano 14 (2020) 7092–7100.
[64] W.B. Liu, L. Xu, T.Z. Bu, H. Yang, G.X. Liu, W.J. Li, Y.K. Pang, C.X. Hu, C. Zhang, T.H. Cheng, Torus structured triboelectric nanogenerator array for water wave energy harvesting, Nano Energy 58 (2019) 499–507.
[65] S.F. Leung, H.C. Fu, M.L. Zhang, A.H. Hassan, T. Jiang, K.N. Salama, Z.L. Wang, J. H. He, Blue energy fuels: Converting ocean wave energy to carbon-based liquid fuels via CO_2 reduction, Energy Environ. Sci. 13 (2020) 1300–1308.
[66] X. Liang, T. Jiang, G.X. Liu, Y.W. Feng, C. Zhang, Z.L. Wang, Spherical triboelectric nanogenerator integrated with power management module for harvesting multidirectional water wave energy, Energy Environ. Sci. 13 (2020) 277–285.
[67] Z.L. Wang, T. Jiang, L. Xu, Toward the blue energy dream by triboelectric nanogenerator networks, Nano Energy 39 (2017) 9–23.
[68] C.S. Wu, W.B. Ding, R.Y. Liu, J.Y. Wang, A.C. Wang, J. Wang, S.M. Li, Y.L. Zi, Z. L. Wang, Keystroke dynamics enabled authentication and identification using triboelectric nanogenerator array, Mater. Today 21 (2018) 216–222.
[69] Y.Q. Liu, E.L. Li, X.M. Wang, Q.Z. Chen, Y.L. Zhou, Y.Y. Hu, G.X. Chen, H.P. Chen, T.L. Guo, Self-powered artificial auditory pathway for intelligent neuromorphic computing and sound detection, Nano Energy 78 (2021), 105403.
[70] B.S. Zhang, Y.J. Tang, R.R. Dai, H.Y. Wang, X.P. Sun, C. Qin, Z.F. Pan, E.J. Liang, Y.C. Mao, Breath-based human-machine interaction system using triboelectric nanogenerator, Nano Energy 64 (2019), 103953.
[71] A. Ahmed, S.L. Zhang, I. Hassan, Z. Saadatnia, Y.L. Zi, J.A. Zu, Z.L. Wang, A washable, stretchable, and self-powered human-machine interfacing Triboelectric nanogenerator for wireless communications and soft robotics pressure sensor arrays, Extreme Mech. Lett. 13 (2017) 25–35.
[72] Z. Wen, M.H. Yeh, H.Y. Guo, J. Wang, Y.L. Zi, W.D. Xu, J.N. Deng, L. Zhu, X. Wang, C.G. Hu, L.P. Zhu, X.H. Sun, Z.L. Wang, Self-powered textile for wearable electronics by hybridizing fiber-shaped nanogenerators, solar cells, and supercapacitors, Sci. Adv. 2 (2016), 1600097.
[73] W.J. Fan, Q. He, K.Y. Meng, X.L. Tan, Z.H. Zhou, G.Q. Zhang, J. Yang, Z.L. Wang, Machine-knitted washable sensor array textile for precise epidermal physiological signal monitoring, Sci. Adv. 6 (2020) 2840.
[74] X. Pu, L.X. Li, M.M. Liu, C.Y. Jiang, C.H. Du, Z.F. Zhao, W.G. Hu, Z.L. Wang, Wearable self-charging power textile based on flexible yarn supercapacitors and fabric nanogenerators, Adv. Mater. 28 (2016) 98–105.
[75] S.S. Kwak, H.J. Yoon, S.W. Kim, Textile-based triboelectric nanogenerators for self-powered wearable electronics, Adv. Funct. Mater. 29 (2019), 1804533.
[76] Y.Q. Yang, N. Sun, Z. Wen, P. Cheng, H.C. Zheng, H.Y. Shao, Y.J. Xia, C. Chen, H. W. Lan, X.K. Xie, C.J. Zhou, J. Zhong, X.H. Sun, S.T. Lee, Liquid-metal-based super-stretchable and structure-designable triboelectric nanogenerator for wearable electronics, ACS Nano 12 (2018) 2027–2034.
[77] X. Peng, K. Dong, C.Y. Ye, Y. Jiang, S.Y. Zhai, R.W. Cheng, D. Liu, X.P. Gao, J. Wang, Z.L. Wang, A breathable, biodegradable, antibacterial, and self-powered electronic skin based on all-nanofiber triboelectric nanogenerators, Sci. Adv. 6 (2020) 9624.
[78] X. Pu, M.M. Liu, X.Y. Chen, J.M. Sun, C.H. Du, Y. Zhang, J.Y. Zhai, W.G. Hu, Z. L. Wang, Ultrastretchable, transparent triboelectric nanogenerator as electronic skin for biomechanical energy harvesting and tactile sensing, Sci. Adv. 3 (2017), 1700015.
[79] G.R. Zhao, Y.W. Zhang, N. Shi, Z.R. Liu, X.D. Zhang, M.Q. Wu, C.F. Pan, H.L. Liu, L.L. Li, Z.L. Wang, Transparent and stretchable triboelectric nanogenerator for self-powered tactile sensing, Nano Energy 59 (2019) 302–310.
[80] H.T. Chen, Y. Song, X.L. Cheng, H.X. Zhang, Self-powered electronic skin based on the triboelectric generator, Nano Energy 56 (2019) 252–268.
[81] Q.B. Guan, Y.H. Dai, Y.Q. Yang, X.Y. Bi, Z. Wen, Y. Pan, Near-infrared irradiation induced remote and efficient self-healable triboelectric nanogenerator for potential implantable electronics, Nano Energy 51 (2018) 333–339.
[82] S.A. Han, J.H. Lee, W. Seung, J. Lee, S.W. Kim, J.H. Kim, Patchable and implantable 2D nanogenerator, Small 17 (2021), 1903519.
[83] B.J. Shi, Z. Li, Y.B. Fan, Implantable energy-harvesting devices, Adv. Mater. 30 (2018), 1801511.
[84] M.A. Parvez Mahmud, N. Huda, S.H. Farjana, M. Asadnia, C. Lang, Recent advances in nanogenerator-driven self-powered implantable biomedical devices, Adv. Energy Mater. 8 (2) (2018), 1701210.
[85] Z.L. Wang, On Maxwell's displacement current for energy and sensors: the origin of nanogenerators, Mater. Today 20 (2017) 74–82.
[86] Z.L. Wang, On the first principle theory of nanogenerators from Maxwell's equations, Nano Energy 68 (2020), 104272.
[87] J.P. Li, H. Huang, T. Morita, Stepping piezoelectric actuators with large working stroke for nano-positioning systems: a review, Sens. Actuators A Phys. 292 (2019) 39–51.
[88] Z.L. Wang, Energy harvesting for self-powered nanosystems, Nano Res. 1 (2008) 1–8.
[89] Z.L. Wang, J.H. Song, Piezoelectric nanogenerators based on zinc oxide nanowire arrays, Science 312 (2006) 242–246.
[90] Z.L. Wang, R. Yang, J. Zhou, Y. Qin, C. Xu, Y. Hu, S. Xu, Lateral nanowire/nanobelt based nanogenerators, piezotronics and piezo-phototronics, Mater. Sci. Eng. R Rep. 70 (2010) 320–329.
[91] Z.Y. Gao, J. Zhou, Y.D. Gu, P. Fei, Y. Hao, G. Bao, Z.L. Wang, Effects of piezoelectric potential on the transport characteristics of metal-ZnO nanowire-metal field effect transistor, J. Appl. Phys. 105 (2009), 113707.
[92] Z.L. Wang, Energy harvesting using piezoelectric nanowires-a correspondence on "energy harvesting using nanowires?" by alexe et al, Adv. Mater. 21 (2009) 1311–1315.
[93] S.H. Wang, L. Lin, Z.L. Wang, Triboelectric nanogenerators as self-powered active sensors, Nano Energy 11 (2015) 436–462.

[94] Z.L. Wang, Triboelectric nanogenerator (TENG)-sparking an energy and sensor revolution, Adv. Energy Mater. 10 (2020), 2000137.
[95] F.R. Fan, Z.Q. Tian, Z.L. Wang, Flexible triboelectric generator, Nano Energy 1 (2012) 328–334.
[96] Z.L. Wang, Triboelectric nanogenerators as new energy technology for self-powered systems and as active mechanical and chemical sensors, ACS Nano 7 (2013) 9533–9557.
[97] Y. Yang, W.X. Guo, K.C. Pradel, G. Zhu, Y.S. Zhou, Y. Zhang, Y.F. Hu, L. Lin, Z. L. Wang, Pyroelectric nanogenerators for harvesting thermoelectric energy, Nano Lett. 12 (2012) 2833–2838.
[98] R. Wang, S. Liu, C.R. Liu, W. Wu, A novel visible light-driven TiO_2 photocatalytic reduction for hexavalent chromium wastewater and mechanism, Water Sci. Technol. J. Int. Assoc. Water Pollut. Res. 83 (2021) 2135–2145.
[99] A.S. Dahiya, F. Morini, S. Boubenia, K. Nadaud, D. Alquier, G. Poulin-Vittrant, Organic/inorganic hybrid stretchable piezoelectric nanogenerators for self-powered wearable electronics, Adv. Mater. Technol. 3 (2018), 1700249.
[100] A. Sultana, T.R. Middya, D. Mandal, ZnS-paper based flexible piezoelectric nanogenerator, AIP Conf. Proc. 1942 (2018), 120018.
[101] Y.F. Lin, J. Song, Y. Ding, S.Y. Lu, Z.L. Wang, Piezoelectric nanogenerator using CdS nanowires, Appl. Phys. Lett. 92 (2008), 022105.
[102] Y.Z. Lei, T.M. Zhao, H.X. He, T.Y. Zhong, H.Y. Guan, L.L. Xing, B.D. Liu, X.Y. Xue, A self-powered electronic-skin for detecting CRP level in body fluid based on the piezoelectric-biosensing coupling effect of GaN nanowire, Smart Mater. Struct. 28 (2019), 105001.
[103] J. Zhang, On the piezotronic behaviours of wurtzite core-shell nanowires, Nanotechnology 31 (2020), 095407.
[104] M.B. Khan, D.H. Kim, J.H. Han, H. Saif, H. Lee, Y. Lee, M. Kim, E. Jang, S.K. Hong, D.J. Joe, T.I. Lee, T.S. Kim, K.J. Lee, Y. Lee, Performance improvement of flexible piezoelectric energy harvester for irregular human motion with energy extraction enhancement circuit, Nano Energy 58 (2019) 211–219.
[105] C.K. Jeong, J.H. Lee, D.Y. Hyeon, Y.G. Kim, S. Kim, C. Baek, G.J. Lee, M.K. Lee, J. J. Park, K.I. Park, Piezoelectric energy conversion by lead-free perovskite $BaTiO_3$ nanotube arrays fabricated using electrochemical anodization, Appl. Surf. Sci. 512 (2020), 144784.
[106] D.Y. Hyeon, K.-I. Park, Piezoelectric flexible energy harvester based on $BaTiO_3$ thin film enabled by exfoliating the mica substrate, Energy Technol. 7 (2019), 1900638.
[107] B. Dudem, D.H. Kim, L.K. Bharat, J.S. Yu, Highly-flexible piezoelectric nanogenerators with silver nanowires and barium titanate embedded composite films for mechanical energy harvesting, Appl. Energy 230 (2018) 865–874.
[108] V. Vivekananthan, A. Chandrasekhara, N.R. Alluri, Y. Purusothaman, W.J. Kim, C. N. Kang, S.J. Kim, A flexible piezoelectric composite nanogenerator based on doping enhanced lead-free nanoparticles, Mater. Lett. 249 (2019) 73–76.
[109] L. Dong, C.S. Wen, Y. Liu, Z. Xu, A.B. Closson, X.M. Han, G.P. Escobar, M. Oglesby, M. Feldman, Z. Chen, J.X.J. Zhang, Piezoelectric buckled beam array on a pacemaker lead for energy harvesting, Adv. Mater. Technol. 4 (2019), 1800335.
[110] W. Yang, W. Han, H. Gao, L. Zhang, S. Wang, L. Xing, Y. Zhang, X. Xue, Self-powered implantable electronic-skin for in situ analysis of urea/uric-acid in body fluids and the potential applications in real-time kidney-disease diagnosis, Nanoscale 10 (2018) 2099–2107.
[111] X. Xue, Z. Qu, Y. Fu, B. Yu, L. Xing, Y. Zhang, Self-powered electronic-skin for detecting glucose level in body fluid basing on piezo-enzymatic-reaction coupling process, Nano Energy 26 (2016) 148–156.
[112] W.L.H. Zhang, L.L. Zhang, H.L. Gao, W.Y. Yang, S. Wang, L.L. Xing, X.Y. Xue, Self-powered implantable skin-like glucometer for real-time detection of blood glucose level In vivo, Nano Micro Lett. 10 (2018) 1–11.
[113] W. Han, H. He, L. Zhang, C. Dong, H. Zeng, Y. Dai, L. Xing, Y. Zhang, X. Xue, A self-powered wearable noninvasive electronic-skin for perspiration analysis based on piezo-biosensing unit matrix of enzyme/ZnO nanoarrays, ACS Appl. Mater. Interfaces 9 (2017) 29526–29537.
[114] H.G. Wei, H. Wang, Y.J. Xia, D.P. Cui, Y.P. Shi, M.Y. Dong, C.T. Liu, T. Ding, J. X. Zhang, Y. Ma, N. Wang, Z.C. Wang, Y. Sun, R.B. Wei, Z.H. Guo, An overview of lead-free piezoelectric materials and devices, J. Mater. Chem. C 6 (2018) 12446–12467.
[115] S.H. Shin, S.Y. Choi, M.H. Lee, J. Nah, High-performance piezoelectric nanogenerators via imprinted sol-gel $BaTiO_3$ nanopillar array, ACS Appl. Mater. Interfaces 9 (2017) 41099–41103.
[116] Q. Zheng, B.J. Shi, Z. Li, Z.L. Wang, Recent progress on piezoelectric and triboelectric energy harvesters in biomedical systems, Adv. Sci. 4 (2017), 1700029.
[117] L. Lu, W. Ding, J. Liu, B. Yang, Flexible PVDF based piezoelectric nanogenerators, Nano Energy 78 (2020), 105251.
[118] A.C. Wang, Z. Liu, M. Hu, C.C. Wang, X.D. Zhang, B.J. Shi, Y.B. Fan, Y.G. Cui, Z. Li, K.L. Ren, Piezoelectric nanofibrous scaffolds as in vivo energy harvesters for modifying fibroblast alignment and proliferation in wound healing, Nano Energy 43 (2018) 63–71.
[119] Y. Yu, H. Sun, H. Orbay, F. Chen, C.G. England, W. Cai, X. Wang, Biocompatibility and in vivo operation of implantable mesoporous PVDF-based nanogenerators, Nano Energy 27 (2016) 275–281.
[120] M.M. Rana, A.A. Khan, G. Huang, N. Mei, R. Saritas, B. Wen, S. Zhang, P. Voss, E. Abdel-Rahman, Z. Leonenko, S. Islam, D. Ban, Porosity Modulated High-performance piezoelectric nanogenerator based on organic/inorganic nanomaterials for self-powered structural health monitoring, ACS Appl. Mater. Interfaces 12 (2020) 47503–47512.
[121] L. Zhang, J. Gui, Z. Wu, R. Li, Y. Wang, Z. Gong, X. Zhao, C. Sun, S. Guo, Enhanced performance of piezoelectric nanogenerator based on aligned nanofibers and three-dimensional interdigital electrodes, Nano Energy 65 (2019), 103924.
[122] J. Fu, Y. Hou, M. Zheng, M. Zhu, Flexible piezoelectric energy harvester with extremely high power generation capability by sandwich structure design strategy, ACS Appl. Mater. Interfaces 12 (2020) 9766–9774.
[123] N.A. Hoque, P. Thakur, P. Biswas, M.M. Saikh, S. Roy, B. Bagchi, S. Das, P.P. Ray, Biowaste crab shell-extracted chitin nanofiber-based superior piezoelectric nanogenerator, J. Mater. Chem. A 6 (2018) 13848–13858.
[124] J. Sun, H. Guo, J. Ribera, C. Wu, K. Tu, M. Binelli, G. Panzarasa, F. Schwarze, Z. L. Wang, I. Burgert, Sustainable and biodegradable wood sponge piezoelectric nanogenerator for sensing and energy harvesting applications, ACS Nano 14 (2020) 14665–14674.
[125] J.B. Yu, X.J. Hou, M. Cui, S.Z. Shi, J. He, Y.W. Sun, C. Wang, X.J. Chou, Flexible PDMS-based triboelectric nanogenerator for instantaneous force sensing and human joint movement monitoring, Sci. China Mater. 62 (2019) 1423–1432.
[126] Z.Q. Bai, Y.L. Xu, Z. Zhang, J.J. Zhu, C. Gao, Y. Zhang, H. Jia, J.S. Guo, Highly flexible, porous electroactive biocomposite as attractive tribopositive material for advancing high-performance triboelectric nanogenerator, Nano Energy 75 (2020), 104884.
[127] G.H. Lim, S.S. Kwak, N. Kwon, T. Kim, H. Kim, S.M. Kim, S.W. Kim, B. Lim, Fully stretchable and highly durable triboelectric nanogenerators based on gold-nanosheet electrodes for self-powered human-motion detection, Nano Energy 42 (2017) 300–306.
[128] H.M. Chen, L. Bai, T. Li, C. Zhao, J.S. Zhang, N. Zhang, G.F. Song, Q.Q. Gan, Y. Xu, Wearable and robust triboelectric nanogenerator based on crumpled gold films, Nano Energy 46 (2018) 73–80.
[129] M.X. Chen, Z. Wang, Y. Zheng, Q.C. Zhang, B. He, J. Yang, M. Qi, L. Wei, Flexible tactile sensor based on patterned Ag-nanofiber electrodes through electrospinning, Sensors 21 (2021) 2413.
[130] C. Xu, A.C. Wang, H.Y. Zou, B.B. Zhang, C.L. Zhang, Y.L. Zi, L. Pan, P.H. Wang, P. Z. Feng, Z.Q. Lin, Z.L. Wang, Raising the working temperature of a triboelectric nanogenerator by quenching down electron thermionic emission in contact-electrification, Adv. Mater. 30 (2018), 1803968.
[131] C.J. Li, Y.Y. Yin, B. Wang, T. Zhou, J.N. Wang, J.J. Luo, W. Tang, R. Cao, Z. Q. Yuan, N.W. Li, X.Y. Du, C.R. Wang, S.Y. Zhao, Y.B. Liu, Z.L. Wang, Self-powered electrospinning system driven by a triboelectric nanogenerator, ACS Nano 11 (2017) 10439–10445.
[132] R. Wang, S. Gao, Z. Yang, Y. Li, W. Chen, B. Wu, W. Wu, Engineered and laser-processed chitosan biopolymers for sustainable and biodegradable triboelectric power generation, Adv. Mater. 30 (2018), 1706267.
[133] G.Z. Li, G.G. Wang, D.M. Ye, X.W. Zhang, Z.Q. Lin, H.L. Zhou, F. Li, B.L. Wang, J. C. Han, High-performance transparent and flexible triboelectric nanogenerators based on PDMS-PTFE composite films, Adv. Electron. Mater. 5 (2019), 1800846.
[134] X.J. Pu, Q. Tang, W.S. Chen, Z.Y. Huang, G.L. Liu, Q.X. Zeng, J. Chen, H.Y. Guo, L. M. Xin, C.G. Hu, Flexible triboelectric 3D touch pad with unit subdivision structure for effective XY positioning and pressure sensing, Nano Energy 76 (2020), 105047.
[135] K. Qin, C. Chen, X.J. Pu, Q. Tang, W.C. He, Y.K. Liu, Q.X. Zeng, G.L. Liu, H.Y. Guo, C.G. Hu, Magnetic array assisted triboelectric nanogenerator sensor for real-time gesture interaction, Nano Micro Lett. 13 (2021) 1–9.
[136] X.P. Chen, X.K. Xie, Y.N. Liu, C. Zhao, M. Wen, Z. Wen, Advances in healthcare electronics enabled by triboelectric nanogenerators, Adv. Funct. Mater. 30 (2020), 2004673.
[137] J.H. Wang, H. Wang, T.Y.Y. He, B.R. He, N.V. Thakor, C. Lee, Investigation of low-current direct stimulation for rehabilitation treatment related to muscle function loss using self-powered TENG system, Adv. Sci. 6 (2019), 1900149.
[138] C. Zhao, H. Feng, L. Zhang, Z. Li, Y. Zou, P. Tan, H. Ouyang, D. Jiang, M. Yu, C. Wang, H. Li, L. Xu, W. Wei, Z. Li, Highly efficient in vivo cancer therapy by an implantable magnet triboelectric nanogenerator, Adv. Funct. Mater. 29 (2019), 1808640.
[139] S. Zhang, J. Xu, J. Yu, L. Song, J. He, N. Ma, X. Hou, X. Chou, An all-rubber-based woven nanogenerator with improved triboelectric effect for highly efficient energy harvesting, Mater. Lett. 287 (2021), 129271.
[140] D. Wang, D. Zhang, Y. Yang, Q. Mi, J. Zhang, L. Yu, Multifunctional latex/polytetrafluoroethylene-based triboelectric nanogenerator for self-powered organ-like mxene/metal-organic framework-derived CuO nanohybrid ammonia sensor, ACS Nano 15 (2021) 2911–2919.
[141] K.K. Fu, Z.Y. Wang, J.Q. Dai, M. Carter, L.B. Hu, Transient electronics: materials and devices, Chem. Mater. 28 (2016) 3527–3539.
[142] L. Yin, X. Huang, H.X. Xu, Y.F. Zhang, J. Lam, J.J. Cheng, J.A. Rogers, Materials, designs, and operational characteristics for fully biodegradable primary batteries, Adv. Mater. 26 (2014) 3879–3884.
[143] Q. Zheng, Y. Zou, Y.L. Zhang, Z. Liu, B.J. Shi, X.X. Wang, Y.M. Jin, H. Ouyang, Z. Li, Z.L. Wang, Biodegradable triboelectric nanogenerator as a life-time designed implantable power source, Sci. Adv. 2 (2016), 1501478.
[144] W. Jiang, H. Li, Z. Liu, Z. Li, J.J. Tian, B.J. Shi, Y. Zou, H. Ouyang, C.C. Zhao, L. M. Zhao, R. Sun, H.R. Zheng, Y.B. Fan, Z.L. Wang, Z. Li, Fully bioabsorbable natural-materials-based triboelectric nanogenerators, Adv. Mater. 30 (2018), 1801895.
[145] H. Ryu, S.W. Kim, Emerging pyroelectric nanogenerators to convert thermal energy into electrical energy, Small 17 (2021), 1903469.
[146] S. Korkmaz, İ.A. Kariper, Pyroelectric nanogenerators (PyNGs) in converting thermal energy into electrical energy: fundamentals and current status, Nano Energy 84 (2021), 105888.

[147] X. Wang, Y. Dai, R. Liu, X. He, S. Li, Z.L. Wang, Light-triggered pyroelectric nanogenerator based on a pn-junction for self-powered near-infrared photosensing, ACS Nano 11 (2017) 8339–8345.
[148] Y. Yang, S.H. Wang, Y. Zhang, Z.L. Wang, Pyroelectric nanogenerators for driving wireless sensors, Nano Lett. 12 (12) (2012) 6408–6413.
[149] H. Karim, M.R.H. Sarker, S. Shahriar, M.A.I. Shuvo, D. Delfin, D. Hodges, T.-L. Tseng, D. Roberson, N. Love, Y. Lin, Feasibility study of thermal energy harvesting using lead free pyroelectrics, Smart Mater. Struct. 25 (2016), 055022.
[150] Q. Leng, L. Chen, H. Guo, J. Liu, G. Liu, C. Hu, Y. Xi, Harvesting heat energy from hot/cold water with a pyroelectric generator, J. Mater. Chem. A 2 (2014) 11940–11947.
[151] F. Gao, W. Li, X. Wang, X. Fang, M. Ma, A self-sustaining pyroelectric nanogenerator driven by water vapor, Nano Energy 22 (2016) 19–26.
[152] Y. Yang, W.X. Guo, K.C. Pradel, G. Zhu, Y.S. Zhou, Y. Zhang, Y.F. Hu, L. Lin, Z. L. Wang, Pyroelectric nanogenerators for harvesting thermoelectric energy, Nano Lett. 12 (2012) 2833–2838.
[153] Y. Yang, Y.S. Zhou, J.M. Wu, Z.L. Wang, Single micro/nanowire pyroelectric nanogenerators as self-powered temperature sensors, ACS Nano 6 (2012) 8456–8461.
[154] Y. Yang, J.H. Jung, B.K. Yun, F. Zhang, K.C. Pradel, W. Guo, Z.L. Wang, Flexible pyroelectric nanogenerators using a composite structure of lead-free KNbO(3) nanowires, Adv. Mater. 24 (2012) 5357–5362.
[155] H. Li, C.S.L. Koh, Y.H. Lee, Y. Zhang, G.C. Phan-Quang, C. Zhu, Z. Liu, Z. Chen, H. Y.F. Sim, C.L. Lay, Q. An, X.Y. Ling, A wearable solar-thermal-pyroelectric harvester: achieving high power output using modified rGO-PEI and polarized PVDF, Nano Energy 73 (2020), 104723.
[156] H. Xue, Q. Yang, D. Wang, W. Luo, W. Wang, M. Lin, D. Liang, Q. Luo, A wearable pyroelectric nanogenerator and self-powered breathing sensor, Nano Energy 38 (2017) 147–154.
[157] T.Y. Zhong, M.Y. Zhang, Y.M. Fu, Y.C. Han, H.Y. Guan, H.X. He, T.M. Zhao, L. L. Xing, X.Y. Xue, Y. Zhang, Y. Zhan, An artificial triboelectricity-brain-behavior closed loop for intelligent olfactory substitution, Nano Energy 63 (2019), 103884.
[158] H. Zeng, H. He, Y. Fu, T. Zhao, W. Han, L. Xing, Y. Zhang, Y. Zhan, X. Xue, A self-powered brain-linked biosensing electronic-skin for actively tasting beverage and its potential application in artificial gustation, Nanoscale 10 (2018) 19987–19994.
[159] G.T. Hwang, Y. Kim, J.H. Lee, S. Oh, C.K. Jeong, D.Y. Park, J. Ryu, H. Kwon, S. G. Lee, B. Joung, D. Kim, K.J. Lee, Self-powered deep brain stimulation via a flexible PIMNT energy harvester, Energy Environ. Sci. 8 (2015) 2677–2684.
[160] S. Lee, H. Wang, Q.F. Shi, L. Dhakar, J.H. Wang, N.V. Thakor, S.C. Yen, C. Lee, Development of battery-free neural interface and modulated control of tibialis anterior muscle via common peroneal nerve based on triboelectric nanogenerators (TENGs), Nano Energy 33 (2017) 1–11.
[161] G. Yao, L. Kang, J. Li, Y. Long, H. Wei, C.A. Ferreira, J.J. Jeffery, Y. Lin, W.B. Cai, X.D. Wang, Effective weight control via an implanted self-powered vagus nerve stimulation device, Nat. Commun. 9 (2018) 5349.
[162] S. Lee, H. Wang, W.Y.X. Peh, N.V. Thakor, S.C. Yen, C. Lee, Direct stimulation of bladder pelvic nerve using battery-free neural clip interface, I. IEEE EMBS C. Neur. E. IEEE, (2019) 706–709.
[163] Z. Li, G.A. Zhu, R.S. Yang, A.C. Wang, Z.L. Wang, Muscle-driven in vivo nanogenerator, Adv. Mater. 22 (2010) 2534–2537.
[164] C. Dagdeviren, B.D. Yang, Y.W. Su, P.L. Tran, P. Joe, E. Anderson, J. Xia, V. Doraiswamy, B. Dehdashti, X. Feng, B.W. Lu, R. Poston, Z. Khalpey, R. Ghaffari, Y.G. Huang, M.J. Slepian, J.A. Rogers, Conformal piezoelectric energy harvesting and storage from motions of the heart, lung, and diaphragm, Proc. Natl. Acad. Sci. 111 (2014) 1927–1932.
[165] B.W. Lu, Y. Chen, D.P. Ou, H. Chen, L.W. Diao, W. Zhang, J. Zheng, W.G. Ma, L. Z. Sun, X. Feng, Ultra-flexible piezoelectric devices integrated with heart to harvest the biomechanical energy, Sci. Rep. 5 (2015) 1–9.
[166] D.H. Kim, H.J. Shin, H. Lee, C.K. Jeong, H. Park, G.T. Hwang, H.Y. Lee, D.J. Joe, J.H. Han, S.H. Lee, J. Kim, B. Joung, K.J. Lee, In vivo self-powered wireless transmission using biocompatible flexible energy harvesters, Adv. Funct. Mater. 27 (2017), 1700341.
[167] X.J. Pu, S.S. An, Q. Tang, H.Y. Guo, C.G. Hu, Wearable triboelectric sensors for biomedical monitoring and human-machine interface, iScience 24 (2021), 102027.
[168] Q. Zheng, H. Zhang, B.J. Shi, X. Xue, Z. Liu, Y.M. Jin, Y. Ma, Y. Zou, X.X. Wang, Z. An, W. Tang, W. Zhang, F. Yang, Y. Liu, X.L. Lang, Z.Y. Xu, Z. Li, Z.L. Wang, In vivo self-powered wireless cardiac monitoring via implantable triboelectric nanogenerator, ACS Nano 10 (2016) 6510–6518.
[169] Y. Ma, Q. Zheng, Y. Liu, B.J. Shi, X. Xue, W.P. Ji, Z. Liu, Y.M. Jin, Y. Zou, Z. An, W. Zhang, X.X. Wang, W. Jiang, Z.Y. Xu, Z.L. Wang, Z. Li, H. Zhang, Self-powered, one-stop, and multifunctional implantable triboelectric active sensor for real-time biomedical monitoring, Nano Lett. 16 (2016) 6042–6051.
[170] H. Ouyang, J.J. Tian, G.L. Sun, Y. Zou, Z. Liu, H. Li, L.M. Zhao, B.J. Shi, Y.B. Fan, Y.F. Fan, Z.L. Wang, Z. Li, Self-powered pulse sensor for antidiastole of cardiovascular disease, Adv. Mater. 29 (2017), 1703456.
[171] H. Ouyang, Z. Liu, N. Li, B.J. Shi, Y. Zou, F. Xie, Y. Ma, Z. Li, H. Li, Q. Zheng, X. C. Qu, Y.B. Fan, Z.L. Wang, H. Zhang, Z. Li, Symbiotic cardiac pacemaker, Nat. Commun. 10 (2019) 1–10.
[172] Z. Liu, Y. Ma, H. Ouyang, B.J. Shi, N. Li, D.J. Jiang, F. Xie, D. Qu, Y. Zou, Y. Huang, H. Li, C.C. Zhao, P.C. Tan, M. Yu, Y.B. Fan, H. Zhang, Z.L. Wang, Z. Li, Transcatheter self-powered ultrasensitive endocardial pressure sensor, Adv. Funct. Mater. 29 (2019), 1807560.
[173] Q. Zheng, B. Shi, F. Fan, X. Wang, L. Yan, W. Yuan, S. Wang, H. Liu, Z. Li, Z. L. Wang, In vivo powering of pacemaker by breathing-driven implanted triboelectric nanogenerator, Adv. Mater. 26 (2014) 5851–5856.
[174] J. Li, L. Kang, Y. Long, H. Wei, Y.H. Yu, Y.H. Wang, C.A. Ferreira, G. Yao, Z. Y. Zhang, C. Carlos, L. German, X.L. Lan, W.B. Cai, X.D. Wang, Implanted battery-free direct-current micro-power supply from in vivo breath energy harvesting, ACS Appl. Mater. Interfaces 10 (2018) 42030–42038.
[175] P.Y. Song, S.Y. Kuang, N. Panwar, G. Yang, D.J.H. Tng, S.C. Tjin, W.J. Ng, M. B. Majid, G. Zhu, K.T. Yong, Z.L. Wang, A self-powered implantable drug-delivery system using biokinetic energy, Adv. Mater. 29 (11) (2017), 1605668.
[176] C.C. Zhao, H.Q. Feng, L.J. Zhang, Z. Li, Y. Zou, P.C. Tan, H. Ouyang, D.J. Jiang, M. Yu, C. Wang, H. Li, L.L. Xu, W. Wei, Z. Li, Highly efficient in vivo cancer therapy by an implantable magnet triboelectric nanogenerator, Adv. Funct. Mater. 29 (2019), 1808640.
[177] Z.R. Liu, J.H. Nie, B. Miao, J.D. Li, Y.B. Cui, S. Wang, X.D. Zhang, G.R. Zhao, Y. B. Deng, Y.H. Wu, Z. Li, L.L. Li, Z.L. Wang, Self-powered intracellular drug delivery by a biomechanical energy-driven triboelectric nanogenerator, Adv. Mater. 31 (2019), 1807795.
[178] M. Bok, Y. Lee, D. Park, S. Shin, Z.J. Zhao, B. Hwang, S.H. Hwang, S.H. Jeon, J. Y. Jung, S.H. Park, J. Nah, E. Lim, J.H. Jeong, Microneedles integrated with a triboelectric nanogenerator: an electrically active drug delivery system, Nanoscale 10 (2018) 13502–13510.
[179] Q. Ouyang, X. Feng, S. Kuang, N. Panwar, P. Song, C. Yang, G. Yang, X. Hemu, G. Zhang, H.S. Yoon, J.P. Tam, B. Liedberg, G. Zhu, K.-T. Yong, Z.L. Wang, Self-powered, on-demand transdermal drug delivery system driven by triboelectric nanogenerator, Nano Energy 62 (2019) 610–619.
[180] Y. Yang, L. Xu, D. Jiang, B.Z. Chen, R. Luo, Z. Liu, X. Qu, C. Wang, Y. Shan, Y. Cui, H. Zheng, Z. Wang, Z.L. Wang, X.D. Guo, Z. Li, Self-powered controllable transdermal drug delivery system, Adv. Funct. Mater. 62 (2021) 610–619.
[181] D.E.J.G.J. Dolmans, D. Fukumura, R.K. Jain, Photodynamic therapy for cancer, Nat. Rev. Cancer 3 (2003) 380–387.
[182] H.E. Lee, J.H. Shin, J.H. Park, S.K. Hong, S.H. Park, S.H. Lee, J.H. Lee, Il-S. Kang, K.J. Lee, Micro light-emitting diodes for display and flexible biomedical applications, Adv. Funct. Mater. 29 (2019), 1808075.
[183] K. Yamagishi, I. Kirino, I. Takahashi, H. Amano, S. Takeoka, Y. Morimoto, T. Fujie, Tissue-adhesive wirelessly powered optoelectronic device for metronomic photodynamic cancer therapy, Nat. Biomed. Eng. 3 (2019) 27–36.
[184] Z. Liu, L. Xu, Q. Zheng, Y. Kang, B. Shi, D. Jiang, H. Li, X. Qu, Y. Fan, Z.L. Wang, Z. Li, Human motion driven self-powered photodynamic system for long-term autonomous cancer therapy, ACS Nano 14 (2020) 8074–8083.
[185] A. Kim, J. Zhou, S. Samaddar, S.H. Song, B.D. Elzey, D.H. Thompson, B. Ziaie, An implantable ultrasonically-powered micro-light-source (microlight) for photodynamic therapy, Sci. Rep. 9 (2019) 1–9.
[186] M. Wu, Z. Zhang, Z. Liu, J. Zhang, Y. Zhang, Y. Ding, T. Huang, D. Xiang, Z. Wang, Y. Dai, X. Wan, S. Wang, H. Qian, Q. Sun, L. Li, Piezoelectric nanocomposites for sonodynamic bacterial elimination and wound healing, Nano Today 37 (2021), 101104.
[187] A. Wang, M. Hu, L. Zhou, X. Qiang, Self-powered well-aligned P(VDF-TrFE) piezoelectric nanofiber nanogenerator for modulating an exact electrical stimulation and enhancing the proliferation of preosteoblasts, Nanomaterials 9 (2019) 349.
[188] S. Du, N. Zhou, Y. Gao, G. Xie, H. Du, H. Jiang, L. Zhang, J. Tao, J. Zhu, Bioinspired hybrid patches with self-adhesive hydrogel and piezoelectric nanogenerator for promoting skin wound healing, Nano Res. 13 (2020) 2525–2533.
[189] W. Tang, J.J. Tian, Q. Zheng, L. Yan, J.X. Wang, Z. Li, Z.L. Wang, Implantable self-powered low-level laser cure system for mouse embryonic osteoblasts proliferation and differentiation, ACS Nano 9 (2015) 7867–7873.
[190] Z. Li, H.Q. Feng, Q. Zheng, H. Li, C.C. Zhao, H. Ouyang, S. Noreen, M. Yu, F. Su, R. P. Liu, L.L. Li, Z.L. Wang, Z. Li, Photothermally tunable biodegradation of implantable triboelectric nanogenerators for tissue repairing, Nano Energy 54 (2018) 390–399.
[191] G. Yao, L. Kang, C. Li, S. Chen, Q. Wang, J. Yang, Y. Long, J. Li, K. Zhao, W. Xu, W. Cai, Y. Lin, X. Wang, A self-powered implantable and bioresorbable electrostimulation device for biofeedback bone fracture healing, Proc. Natl. Acad. Sci. USA 118 (2021), e2100772118.
[192] Y. Zhang, L. Xu, Z. Liu, X. Cui, Z. Xiang, J. Bai, D. Jiang, J. Xue, C. Wang, Y. Lin, Z. Li, Y. Shan, Y. Yang, L. Bo, Z. Li, X. Zhou, Self-powered pulsed direct current stimulation system for enhancing osteogenesis in MC3T3-E1, Nano Energy 85 (2021), 106009.
[193] J. Tian, R. Shi, Z. Liu, H. Ouyang, M. Yu, C. Zhao, Y. Zou, D. Jiang, J. Zhang, Z. Li, Self-powered implantable electrical stimulator for osteoblasts' proliferation and differentiation, Nano Energy 59 (2019) 705–714.
[194] Y. Chen, G. Gao, J. Zhao, H. Zhang, J. Yu, X. Yang, Q. Zhang, W. Zhang, S. Xu, J. Sun, Y. Meng, Q. Sun, Piezotronic graphene artificial sensory synapse, Adv. Funct. Mater. 29 (2019), 1900959.
[195] J.R. Yu, X.X. Yang, G.Y. Gao, Y. Xiong, Y.F. Wang, J. Han, Y.H. Chen, H. Zhang, Q. J. Sun, Z.L. Wang, Bioinspired mechano-photonic artificial synapse based on graphene/MoS_2 heterostructure, Sci. Adv. 7 (2021), eabd9117.
[196] J. Yu, G. Gao, J. Huang, X. Yang, J. Han, H. Zhang, Y. Chen, C. Zhao, Q. Sun, Z. L. Wang, Contact-electrification-activated artificial afferents at femtojoule energy, Nat. Commun. 12 (2021) 1–10.

[197] C. Deng, W. Tang, L. Liu, B. Chen, M. Li, Z.L. Wang, Self -powered insole plantar pressure mapping system, Adv. Funct. Mater. 28 (2018), 1801606.
[198] K. Dong, J. Deng, W. Ding, A.C. Wang, P. Wang, C. Cheng, Y.C. Wang, L. Jin, B. Gu, B. Sun, Z.L. Wang, Versatile core–sheath yarn for sustainable biomechanical energy harvesting and real-time human-interactive sensing, Adv. Energy Mater. 8 (2018), 1801114.
[199] C. Li, D. Liu, C. Xu, Z. Wang, S. Shu, Z. Sun, W. Tang, Z.L. Wang, Sensing of joint and spinal bending or stretching via a retractable and wearable badge reel, Nat. Commun. 12 (2021) 2950.